Journal of Sound and Vibration 327 (2009) 368–390

Contents lists available at ScienceDirect

Journal of Sound and Vibration

journal homepage: www.elsevier.com/locate/jsvi

# Identification of damaged shafts using active sensing—Simulation and experimentation

José M. Machorro-López [a,*], Douglas E. Adams [a,1], Julio C. Gómez-Mancilla [b], Kamran A. Gul [a]

[a] Ray W. Herrick Laboratories, School of Mechanical Engineering, Purdue University, 140 S. Martin Jischke Drive, West Lafayette, IN 47907-2031, USA
[b] Laboratory of Vibrations and Rotordynamics ESIME, Instituto Politécnico Nacional, Edificio Z-4, 2do. Piso, U.P. Adolfo López Mateos, Col. Lindavista, C.P. 07738, Mexico City, Mexico

ARTICLE INFO

*Article history:*
Received 15 January 2008
Received in revised form
17 June 2009
Accepted 25 June 2009
Handling Editor: C.L. Morfey
Available online 3 August 2009

ABSTRACT

Rotating machines are susceptible to fatigue failures if transverse cross-sectional cracks form in shafts. Early detection of cracks is essential to avoid a catastrophic event and the associated costs. In this work, a detailed physics-based three-dimensional model of an experimental Machinery Fault Simulator® apparatus is developed using ANSYS® with beam elements based on Timoshenko beam theory. Different kinds of faults such as transverse cracks, imbalance, misalignment, bent shafts, and combinations thereof are considered. Off-line and on-line experimental tests are carried out. Different types of external excitation with piezoelectric actuators are introduced and the vibration responses in several dimensions are measured. Numerical and experimental results demonstrate that there are only subtle changes in the passive vibration natural frequencies and mode shapes due to cracks in the shaft; therefore, active sensing is necessary to detect damage. It is also shown that torsional and axial responses that are measured using active vibration sensing are highly sensitive to cracks in the shaft.


## 1. Introduction

### 1.1. General

Shafts are components subjected to difficult operating conditions in high-performance rotating equipment such as compressors, steam and gas turbines, generators, pumps, and engines that are used in process and utility plants. Rotating machines are being designed to operate at higher mechanical efficiencies by decreasing the weight and dimensional tolerances leading to greater operating speeds, power transfer, loads, and stresses. As a consequence, many rotordynamic systems contain shafts that are susceptible to fatigue failure due to transverse cross-sectional cracks. The wide variations in temperature and environment during operation also contribute to conditions conducive to fatigue failure.

The fracture of a turbine shaft due to cracking is a rare event; however, if a cracked shaft is not detected and bursts, the consequences are dire. Several power plants around the world have experienced accidents due to burst shafts. Personal

* Corresponding author. Tel.: +1 765 413 8351; fax: +1 765 494 0787.
*E-mail addresses:* machorrolopez@yahoo.com.mx, jmachorr@purdue.edu (J.M. Machorro-López), deadams@purdue.edu (D.E. Adams), jcgomez@ipn.mx (J.C. Gómez-Mancilla), kgul@purdue.edu (K.A. Gul).
*URLs:* http://widget.ecn.purdue.edu/~FEND2 (D.E. Adams), http://www.esimez.ipn.mx/labrotomecanica/mx.geocities.com/armandozam/index.html (J.C. Gómez-Mancilla).
[1] Tel.: +1 765 449 4249; fax: +1 765 494 0787.

0022-460X/$ - see front matter © 2009 Elsevier Ltd. All rights reserved.
doi:10.1016/j.jsv.2009.06.025

**Nomenclature**

| | |
|---|---|
| $A_f$ | cross-sectional area of the damaged section |
| $A_i$ | cross-sectional area of the healthy section |
| $B1$ | left side bearing (inboard) |
| $B1_{i,j,k}$ | stiffness and damping in $B1$ |
| $B2$ | right side bearing (outboard) |
| $B2_{i,j,k}$ | stiffness and damping in $B2$ |
| $C1$ | transverse crack between $B1$ and $D1$ |
| $C2$ | transverse crack between $D1$ and $D2$ |
| $C3$ | transverse crack between $D2$ and $B2$ |
| $d$ | diameter |
| $D1$ | left side disc (inboard) |
| $D2$ | right side disc (outboard) |
| $E$ | Young's modulus |
| $F_x$ | axial excitation force |
| $F_y$ | vertical excitation force |
| $F_z$ | horizontal excitation force |
| $g$ | gravity |
| $I_{as}$ | moment of inertia of the angular sector OADCO |
| $I_f$ | moment of inertia of the damaged circular section |
| $I_i$ | moment of inertia of the healthy circular section |
| $I_{ts}$ | moment of inertia of the triangular sector OABCO |
| $J_f$ | polar moment of inertia of the damaged circular section |
| $J_i$ | polar moment of inertia of the healthy circular section |
| $l_{\text{shaft}}$ | shaft length between bearings |
| $L$ | length |
| $L_{\text{shaft}}$ | total length of the shaft |
| $M_x$ | torsional excitation moment around $X$ |
| $M_y$ | torsional excitation moment around $Y$ |
| $M_z$ | torsional excitation moment around $Z$ |
| OABCD | points describing the crack geometry |
| $p$ | crack depth |
| $p/d_{\text{shaft}}$ | relative crack depth |
| $r$ | shaft radius |
| $S1$ | left side foundation (inboard) |
| $S1_{i,j,k}$ | stiffness and damping in $S1$ |
| $S2$ | right side foundation (outboard) |
| $S2_{i,j,k}$ | stiffness and damping in $S2$ |
| $t_{\text{crack}}$ | crack thickness |
| $T_x$ | torsional vibratory response around $X$ |
| $T_y$ | torsional vibratory response around $Y$ |
| $T_z$ | torsional vibratory response around $Z$ |
| $U_x$ | axial vibratory response |
| $U_y$ | vertical vibratory response |
| $U_z$ | horizontal vibratory response |
| $w_d$ | length between discs |
| $W$ | weight |
| $X,Y,Z$ | Cartesian coordinates |
| $\alpha$ | angle between $A$ and $B$ |
| $\theta_f$ | angle between $Z$-axis and $C$ |
| $\theta_i$ | angle between $Z$-axis and $A$ |
| $\theta_m$ | angle between $Z$-axis and $B$ (crack orientation) |
| $v$ | Poisson's ratio |
| $\rho$ | density |
| $\omega_c$ | first critical speed considering rigid bearings |

safety, operating costs, and increasing overhaul-time intervals motivate research in cracked shaft detection. Vibration monitoring is one approach for detecting cracks that could be implemented in an automated manner to help alleviate cost and safety issues.

Several catastrophic events involving cracked shaft bursts have taken place in different power plants around the world. Some examples of these events are the recent destruction of a 300 MW turboset at the Kashira power station in Russia in 2002 [1]; the steam turbine explosion at the Tennessee Valley Authority Gallatin No. 2 power plant in the United States of America in 1974 [2]; and the accident in 1988 in Germany due to a 330 MW steam turboset explosion [3].

The Electric Power Research Institute estimates direct and indirect losses (repair, replacement, and loss of revenue) at around 1 billon US dollars in the conventional and nuclear power industry alone. To ensure that rotating machinery is not damaged, operators commonly use on-line (while the shaft is rotating) vibratory monitoring of the bearings. However, it is difficult to detect shaft cracks due to the special nature of this kind of fault.

The aim of this paper is to present and interpret the results of an extensive numerical and experimental study that can be used for detecting damaged non-rotating shafts (off-line case) and damaged rotating shafts (on-line case) by analyzing the coupled vibratory response obtained by implementing different kinds of external excitations. The results show that it is important to use torsional and axial transducers (sensors and possibly actuators as well) because torsional and axial vibratory responses are sensitive to cracked shafts.

### 1.2. Literature review

During the last three decades, researchers have studied methods to detect cracked shafts in rotating machinery. The thorough review paper written by Sabnavis et al. [4] covers many aspects of this problem.

It is known that the presence of faults somewhat alters the vibrational characteristics of rotordynamic systems, and therefore, those variations have often been used to detect damage in rotating machinery. Most fault diagnosis techniques that have been proposed so far based on vibration monitoring consist of a comparison of the operational vibratory response without the incorporation of any additional external excitation. These techniques have also focused only on measurements

in two degrees of freedom (DOF; vertical and horizontal) at the bearing locations of the rotordynamic system. Data are first acquired when the system is started up for first time (baseline) and is compared to data from the machine when it is suspected of being faulty. In this way, the differences in vibratory behavior can be used to determine the presence of at least one fault in the machinery. By tracking this fault, statistical models can then be used to predict the likelihood of failure based on the findings of studies conducted by industry and researchers.

The most common faults that can occur in rotating machinery, such as imbalance, misalignment, bent shafts, etc., are the least difficult to detect and they are extensively documented in the literature. The diagnosis procedure described above has been successfully applied for these faults because the vibratory measurements obtained in just two directions are usually adequate to detect those faults. Moreover, many researchers have obtained similar or identical conclusions in their corresponding studies. In contrast, the specific case of cracks in rotating shafts is more difficult to diagnose. There is no general agreement regarding the characteristic vibratory tendencies of this kind of damage. Some researchers report that changes in natural frequencies and/or mode shapes can be used to detect cracks, whereas other researchers report contradictory findings. Many researchers have proposed the vibration amplitudes at the $1\times$ and/or $2\times$ frequency components as indicators of cracks in shafts, but other many researchers disagree with this proposal, indicating that imbalance and misalignment are common faults whose effects are more evident at those frequency components, thereby masking the crack. Similarly, a group of researchers has presented techniques for crack detection by analyzing the peaks of vibratory amplitudes occurring at higher frequency components ($3\times$, $4\times$, etc.); however, another group reports that these amplitudes are highly damped; consequently, the high-frequency amplitudes are too small, making it difficult to detect the crack.

These discrepancies can be attributed to the fact that a crack in a shaft is a complex phenomenon. By using only operational vibration measurements in two degrees of freedom, the ability to detect cracking is compromised. Consequently, our research discusses numerical and experimental results obtained using active sensing along with an external excitation applied to a bearing.

Dimarogonas combined fracture mechanics with rotordynamics to calculate the full local compliance matrix due to a crack. If the crack opens and closes, depending on the rotation and vibration amplitude, then the system is nonlinear and coupled vibrations appear due to the crack. This phenomenon was reported for the first time by Papadopoulos and Dimarogonas [5] for longitudinal and bending vibrations and also for bending and torsional vibrations.

Rao [6] detected that in cracked horizontal rotating shafts, excitations appear at the fundamental critical frequency but also at both supersynchronous and subsynchronous frequencies. In experimental research related to cracked shafts, many authors have linked theories in rotordynamics and fracture mechanics to crack detection. For example, Bently [7] and Muszynska [8] have primarily used vibration data to detect cracks. Nilsson [9] suggested that just the $1\times$ and $2\times$ frequency components should be analyzed in rotating systems to detect cracks because the higher harmonics are highly damped.

An interesting survey about the stability behavior of a cracked Laval rotor and of the forced vibrations due to both the imbalance and the crack was given by Gasch [10] in 1993. He presented stability plots showing the stability regions of a shaft with a transverse crack and described several strategies to detect this damage.

A numerical model of a shaft with two transverse open cracks was developed by Sekhar [11], who reported significant eigenfrequency changes for shafts having low slenderness ratios. If two cracks have unequal depths, the larger crack was shown to primarily affect the eigenfrequencies and the effect of even small cracks on the stability speed was evident in the results.

Darpe et al. [12] studied the effect of two transverse cracks in a shaft. They calculated the flexibility of the shaft due to these two cracks and reported that the relative positions and orientations of the cracks notably changed the dynamic response.

Penny and Friswell [13] analyzed simplified models for shaft cracks. They concluded that the simple harmonic crack breathing function as proposed by Mayes enables linear modeling, which yields similar responses to the more involved class of nonlinear models.

With numerical simulations and experiments, Gómez-Mancilla and his research group have proposed the analysis of three aspects to facilitate cracked shaft detection: vibratory response at local resonances (vibration peaks occurring at rational fractions of the fundamental rotating critical speed) using discrete Fourier transform and Bode plots; orbital evolution around 1/2, 1/3, and 1/4 of the critical speed [14]; and the variation in the threshold of vibratory stability for various crack-imbalance orientations [15]. They also found in [16] that different mathematical models of the crack breathing mechanism affect the vibratory responses of the system.

Moreover, Kucherenko and Gómez-Mancilla [17] performed a nonlinear analysis and they established that rotordynamic coefficients at shaft mid-span location have a very strong influence as compared with rotordynamic coefficients at the end bearing supports.

A simple model proposed by Al-Said et al. [18] described the flexural vibration characteristics of a cracked rotating Timoshenko beam. The cracked beam was modeled using two uniform segments connected by a torsional spring at the crack location.

Interesting methods to detect faults have been proposed by Randall, Lees and their teams. Antoni and Randall [19] demonstrated how the spectral kurtosis can be efficiently used in the vibration-based condition monitoring of rotating machines to detect incipient faults even in the presence of strong masking noise. On the other hand, Sinou and Lees [20]

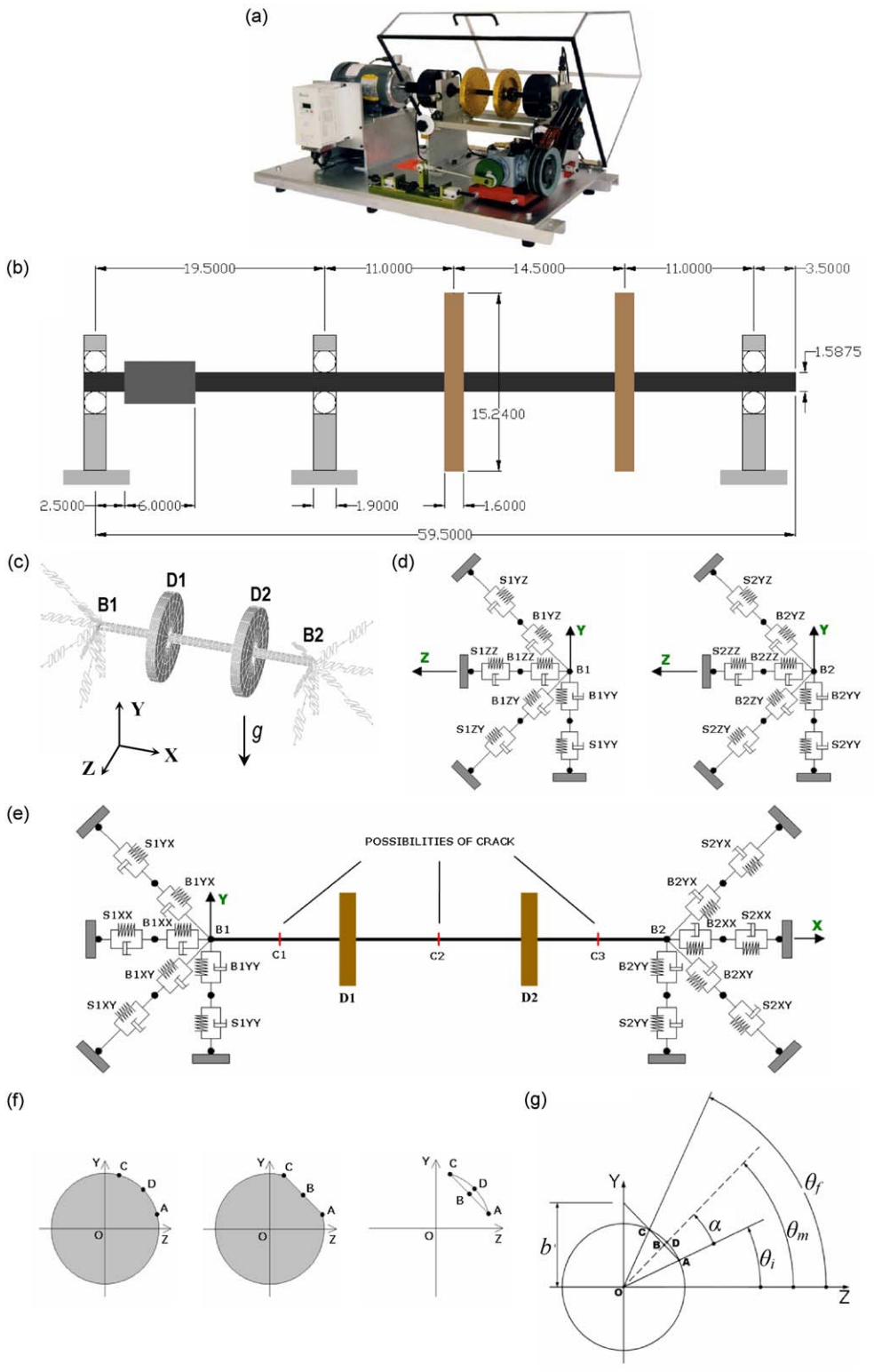


**Fig. 1.** (a) Machinery Fault Simulator (MFS). (b) MFS schematic with units in cm. (c) Final ANSYS® model and reference system. (d) Coefficients of the *YZ*-plane using the ANSYS® model. (e) ANSYS® model with representation in the *XY*-plane. (f) Model of the crack: healthy transverse section, cracked transverse section, and reduction in the shaft transverse section due to the crack. (g) Geometric characteristics of the crack.

**Table 1**
Change of the shaft geometric characteristics due to the crack.

| Relative crack depth $p/d_{\text{shaft}}$ | Final cross-sectional area $A_f$ ($10^{-4}$ m$^2$) | Crack orientation $\theta_m$ (deg) | Final moment of inertia $I_f$ ($10^{-9}$ m$^4$) | Final polar moment of inertia $J_f$ ($10^{-9}$ m$^4$) | $I$ and $J$ reduction (%) |
|---|---|---|---|---|---|
| 0.000 | 1.9793 | – | 3.1176 | 6.2353 | 0.00 |
| 0.125 | 1.8365 | 0, 180 | 3.0363 | 6.0726 | 2.61 |
| 0.125 | 1.8365 | 45, 135, 225, 315 | 2.7491 | 5.4982 | 11.82 |
| 0.125 | 1.8365 | 90, 270 | 2.4620 | 4.9239 | 21.03 |
| 0.250 | 1.5924 | 0, 180 | 2.7230 | 5.4460 | 12.66 |
| 0.250 | 1.5924 | 45, 135, 225, 315 | 2.2933 | 4.5866 | 26.44 |
| 0.250 | 1.5924 | 90, 270 | 1.8636 | 3.7271 | 40.22 |
| 0.500 | 0.9897 | 0, 180 | 1.5588 | 3.1176 | 50.00 |
| 0.500 | 0.9897 | 45, 135, 225, 315 | 1.5588 | 3.1176 | 50.00 |
| 0.500 | 0.9897 | 90, 270 | 1.5588 | 3.1176 | 50.00 |

Initial cross-sectional area $= A_i = 1.9793\text{e}{-4}\,\text{m}^2$; initial moment of inertia $= I_i = 3.1176\text{e}{-9}\,\text{m}^4$; initial polar moment of inertia $= J_i = 6.2353\text{e}{-9}\,\text{m}^4$.

obtained some distinguishing features of a cracked rotor by examining the evolution of the first critical speed, associated amplitudes at the critical speed and half of the critical speed, and the resulting orbits during transient operation. Recently, various types of nonlinear resonances of a Jeffcott rotor with a crack were investigated both numerically and experimentally by Ishida and Inoue [21]; the system was harmonically excited.

The work presented in this paper differs from these previous works by focusing on longitudinal and torsional vibration responses as a means of detecting cracks. Experiments and simulations are performed using a piezoelectric actuator on one bearing housing to stimulate responses that are then measured using triaxial accelerometers on the other bearing housing. The external excitation produces a strong coupled vibratory response in various degree of freedom when a crack exists. As a result, it is proposed that damage can be more easily detected using active sensing.

## 2. Numerical model

A bench top Machinery Fault Simulator (MFS) made by Spectra Quest® (with two ball bearings) was used as the experimental apparatus and as the basis for developing the physics-based model in this work. Fig. 1(a) is a photograph of the MFS, where the motor, shaft, discs, and bearing housings are evident. Fig. 1(b) shows the dimensions of the MFS setup. The shaft can be removed, cracks can be seeded using electro-discharge machining, and then shafts can be replaced in the MFS for operational testing.

ANSYS® was used to develop a detailed physics-based three-dimensional (3-D) model of the MFS. Several types of faults in real machinery can be simulated with this numerical model and experimentally validated with the MFS (refer to Fig. 1(c)). More details about the numerical model can be found in the Appendix, Figs. 1(d)–(g), and Table 1.

## 3. Numerical results and analysis

To determine the feasibility of detecting cracks in shafts by analyzing the change in natural frequencies and modal shapes due to cracking, the first task with the numerical model was to obtain these modal parameters (natural frequencies and modal shapes) for a system with a healthy shaft and a system with various faults: open deep crack ($p/d_{\text{shaft}} = 0.50$) at the mid-span, combined misalignment, and bent shaft (see Fig. 2). The results indicate that there are no significant changes in the natural frequencies due to a cracked shaft or bent shaft; and the modal shapes are similar for all the cases, except for the case of combined misalignment, which exhibits interesting differences at several frequencies. A deep crack was considered, and detection was not possible using shifts in modal properties. Next, other methods of detection were considered: (1) passive measurements of more than one vibration response in more than one direction and (2) higher frequency active measurements of responses that are stimulated using piezoelectric actuators attached at the bearings.

### 3.1. Transverse and axial excitation

Transverse and axial excitations on bearing 1 from 0 to 10 kHz were applied in the healthy and damaged shaft and the coupled vibratory response was analyzed on the opposite bearing. Three cases of cracks at the mid-span were considered: an open incipient crack ($p/d_{\text{shaft}} = 0.125$), and both open and closed deep cracks ($p/d_{\text{shaft}} = 0.50$); however, the results for all the off-line cases (including also torsional excitations) were found to be identical for open and closed deep cracks; that is, the orientation of the crack did not influence the vibratory response when a non-rotating shaft was considered, and therefore, in the interests of brevity, the off-line response for closed deep cracks will not be presented. Whereas for on-line cases (shaft with rotation), the responses for open and closed deep cracks are always different only in the axial direction, and in order to justify this finding, only one plot for a closed deep crack will be shown in Section 3.2.2. Black circles indicate


**Fig. 2.** Numerically generated mode shapes and natural frequencies (modes 1–6) for (a) a healthy shaft, (b) a cracked shaft, (c) combined misalignment, and (d) a bent shaft.

the response(s) that is (are) sensitive to a fault when in the same plot there are several curves that are not altered by the presence of the fault.

### *3.1.1. Harmonic analysis at 0 rev/min (off-line)*

The advantage of using a horizontal excitation was evident as shown in Figs. 3(g)–(i) because changes in torsional response ($T_x$) were observed for all the cases with a damaged shaft. The vertical excitation produced a small axial response for an open incipient crack (Figs. 3(a)–(c)), and the axial excitation was not useful for damage detection because it did not differ for healthy and cracked shafts (Figs. 3(d)–(f)). It has been shown that an external excitation can be used with the

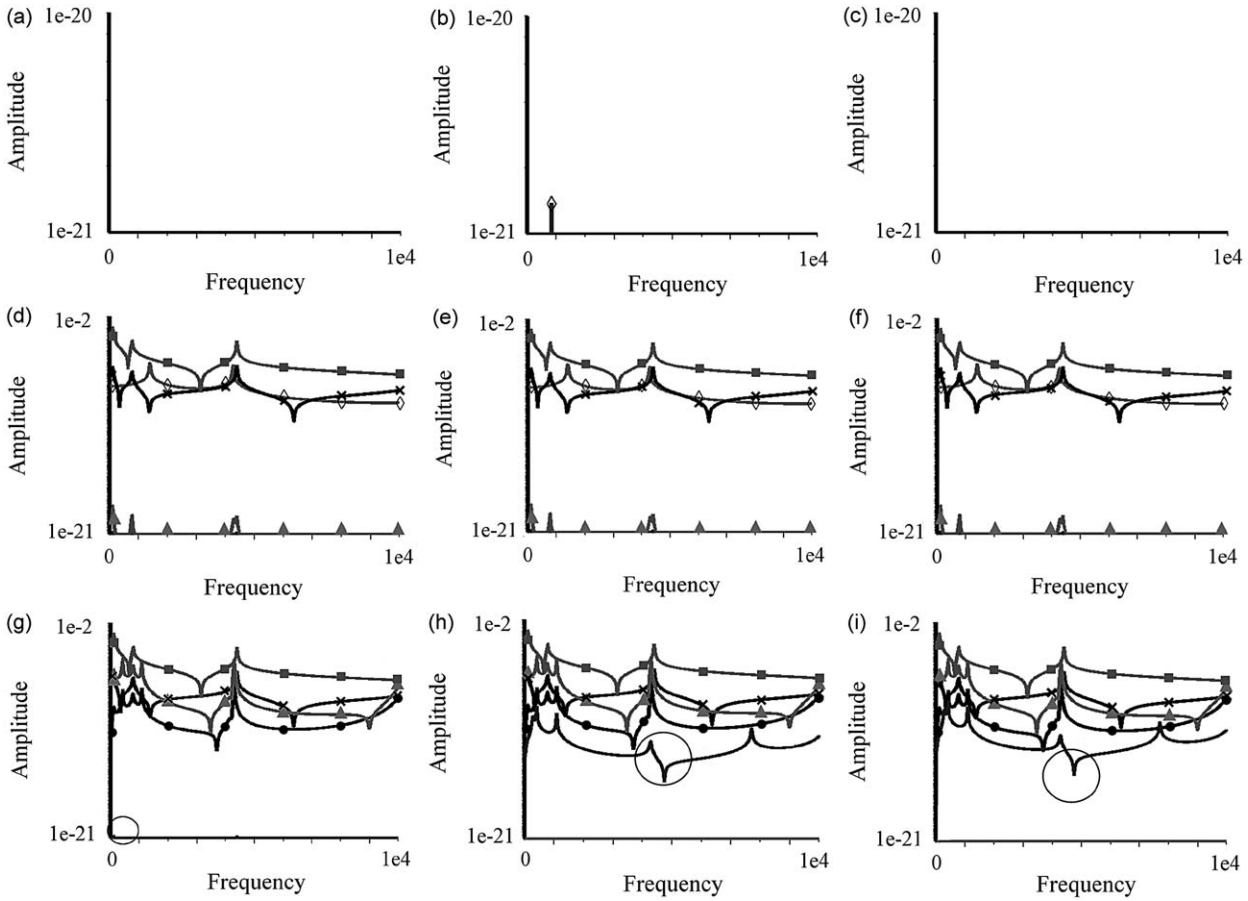


**Fig. 3.** Off-line amplitude vs. frequency (Hz) plots for transverse and axial excitation on bearing 1 and responses on bearing 2. (a) Healthy shaft, vertical excitation. (b) Open incipient crack, vertical excitation. (c) Open deep crack, vertical excitation. (d) Healthy shaft, axial excitation. (e) Open incipient crack, axial excitation. (f) Open deep crack, axial excitation. (g) Healthy shaft, horizontal excitation. (h) Open incipient crack, horizontal excitation. (i) Open deep crack, horizontal excitation. $U_x$ (◇), $U_y$ (✖), $U_z$ (●), $T_x$ (——), $T_y$ (▲), $T_z$ (■).

system off-line to detect certain kinds of cracks; however, the potential for using external excitations is greater when the analysis is performed on-line for a rotating shaft. Results for an operating speed of 5000 rev/min are discussed next.

### 3.1.2. *Harmonic analysis at 5000 rev/min (on-line)*

The most important aspect of the on-line simulation result was the notable torsional response about the *X*-axis for all the cases considering a cracked shaft with an excitation in any orientation (Fig. 4). This result was useful from a diagnostic point of view because the torsional response ($T_x$) was almost zero for a healthy shaft. Additionally, the axial response again provided a means to detect damage mainly for the case where a vertical excitation was applied (Figs. 4(a)–(c)). The amplitudes for the incipient and deep crack responses that differ from the case for a healthy shaft were always somewhat larger for a deep crack than for the incipient crack, except the axial amplitudes, which did not exhibit a clear tendency in this aspect for all the studied cases. When $U_x$ components are very small, they are plotted separately below other plots as in parts (a)–(c) and (g)–(i) of Fig. 4.

The useful responses for detecting cracks are summarized in Table 2(a) for each type of excitation. The torsional response ($T_x$) and the axial response were the most useful for detecting cracks. The torsional response ($T_x$) was the preferred option to detect damage because its amplitudes were significant whereas the axial amplitudes were relatively small.

When the same types of plots were generated without external excitation with the shaft rotating at 5000 rev/min, there was also a considerable reduction in the torsional response ($T_x$) for a cracked shaft. Moreover, different axial responses were again obtained for healthy and cracked shafts. In this case, the crack inhibited the small axial amplitude peak that existed for a healthy shaft (Fig. 5). The importance of the axial response without any external excitation is also validated in the experimental portion of this paper. Both of the useful response measurements for detecting cracks without external

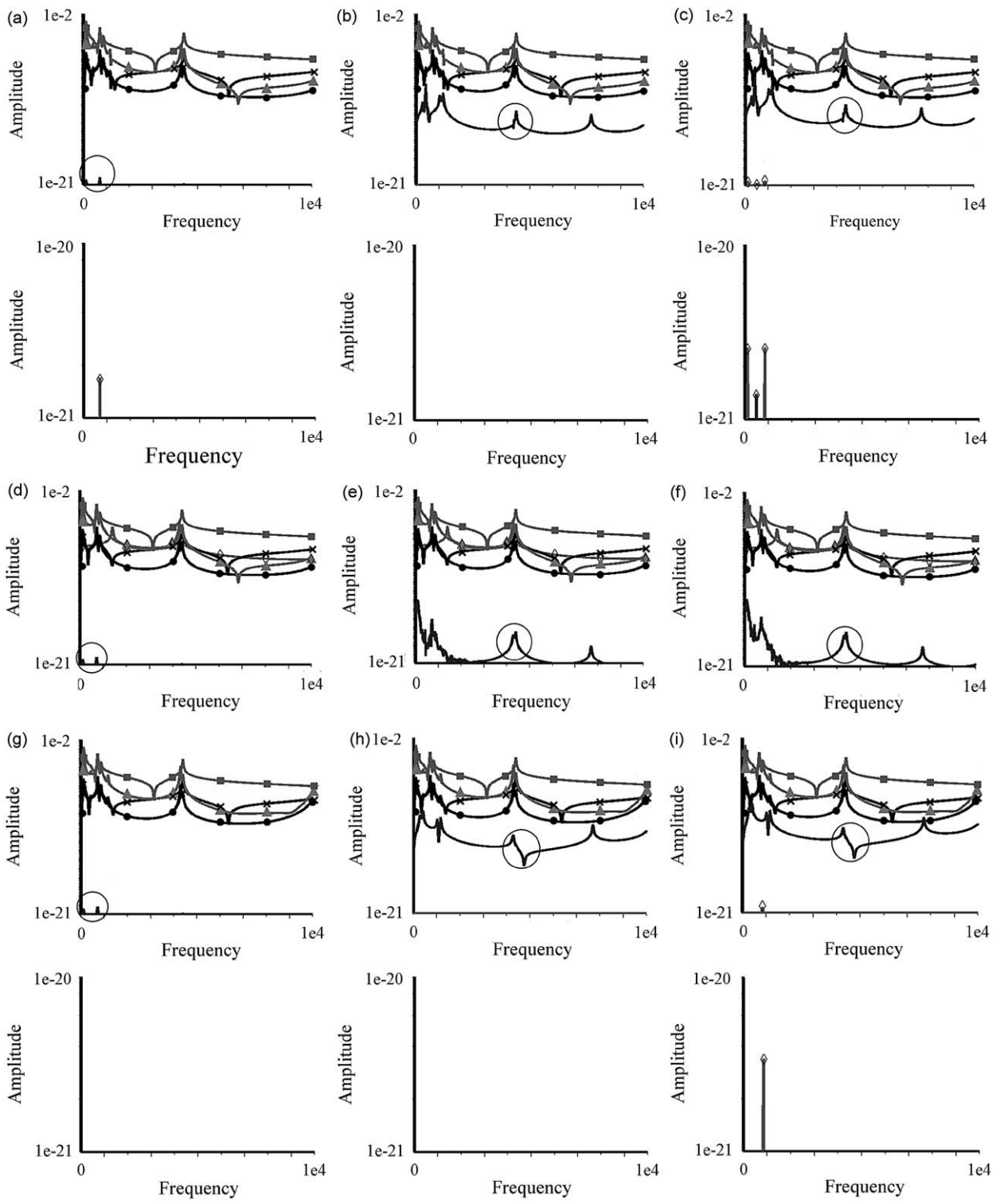


**Fig. 4.** On-line amplitude vs. frequency (Hz) plots for transverse and axial excitation on bearing 1 and responses on bearing 2. (a) Healthy shaft, vertical excitation. (b) Open incipient crack, vertical excitation. (c) Open deep crack, vertical excitation. (d) Healthy shaft, axial excitation. (e) Open incipient crack, axial excitation. (f) Open deep crack, axial excitation. (g) Healthy shaft, horizontal excitation. (h) Open incipient crack, horizontal excitation. (i) Open deep crack, horizontal excitation. When $U_x$ components are very small, they are plotted separately below other plots as in parts (a)–(c) and (g)–(i). $U_x$ (◇), $U_y$ (✖), $U_z$ (●), $T_x$ (——), $T_y$ (▲), $T_z$ (■).

**Table 2**
Summary of crack detection with external excitation.

| Simulation case | Type of excitation | **Useful responses for detecting cracks** | | |
|---|---|---|---|---|
| | | Open incipient crack | Open deep crack | Closed deep crack |
| *(a) Summary of crack detection with transverse or axial excitation* | | | | |
| Off-line | $-F_y$ | $U_x$ | – | – |
| Off-line | $-F_x$ | – | – | – |
| Off-line | $-F_z$ | $T_x$ | $T_x$ | $T_x$ |
| On-line | $-F_y$ | $T_x$, $U_x$ | $T_x$, $U_x$ | $T_x$, $U_x$ |
| On-line | $-F_x$ | $T_x$ | $T_x$ | $T_x$ |
| On-line | $-F_z$ | $T_x$ | $T_x$, $U_x$ | $T_x$, $U_x$ |
| *(b) Summary of crack detection with torsional excitation* | | | | |
| Off-line | $-M_x$ | $U_z$, $T_y$ | $U_z$, $T_y$ | $U_z$, $T_y$ |
| Off-line | $-M_y$ | $T_x$ | $T_x$ | $T_x$ |
| Off-line | $-M_z$ | $U_x$ | $U_x$ | $U_x$ |
| On-line | $-M_x$ | $U_z$, $U_x$, $T_y$ | $U_z$, $U_x$, $T_y$ | $U_z$, $U_x$, $T_y$ |
| On-line | $-M_y$ | $T_x$, $U_x$ | $T_x$, $U_x$ | $T_x$, $U_x$ |
| On-line | $-M_z$ | $T_x$, $U_x$ | $T_x$, $U_x$ | $T_x$, $U_x$ |

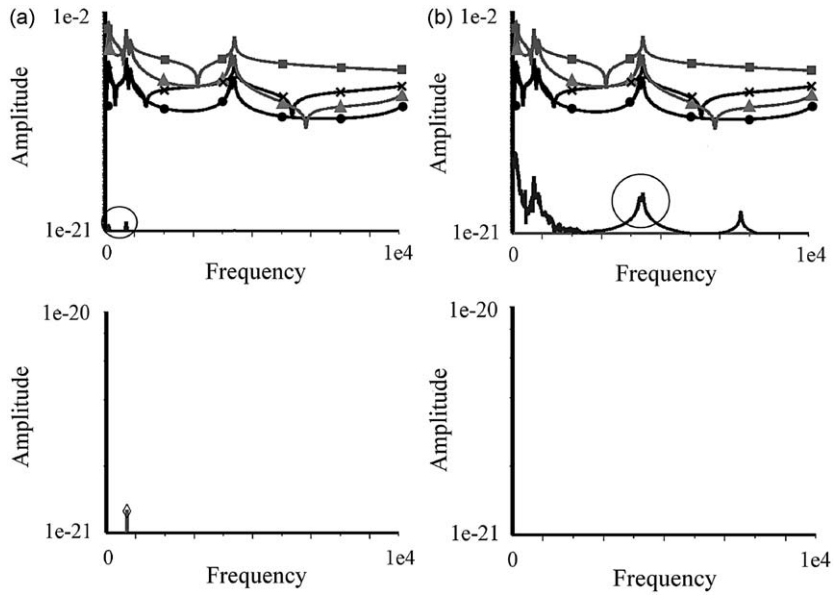


**Fig. 5.** On-line amplitude vs. frequency (Hz) plots without excitation, responses on bearing 2. (a) Healthy shaft. (b) Open incipient crack. When $U_x$ components are very small, they are plotted separately below other plots as in parts (a) and (b). $U_x$ (◇), $U_y$ (✖), $U_z$ (●), $T_x$ (——), $T_y$ (▲), $T_z$ (■).

excitation would be too small to detect cracks in practice due to measurement variability; therefore, it is believed that an external excitation would be needed.

### 3.2. Torsional excitation

A torsional excitation from 0 to 10 kHz was also studied; however, the most relevant torsional excitation is when the torsional impulse is applied about the *X*-axis because it would be too complicated to provide a torsional excitation around either the *Y*- or *Z*-axis. Despite these practical limitations, torsional responses about the *X*-axis were obtained for a cracked shaft when a torsional excitation was applied about either the *Y*- or *Z*-axis.

#### 3.2.1. Harmonic analysis at 0 rev/min (off-line)

For a torsional excitation, the crack orientation did not influence the vibratory response of a non-rotating shaft, as mentioned previously. The horizontal response obtained with a torsional excitation about the *X*-axis was the most sensitive to cracking (Figs. 6(a)–(c)). This type of measurement would be feasible in practice. Additionally, the torsional response ($T_x$)

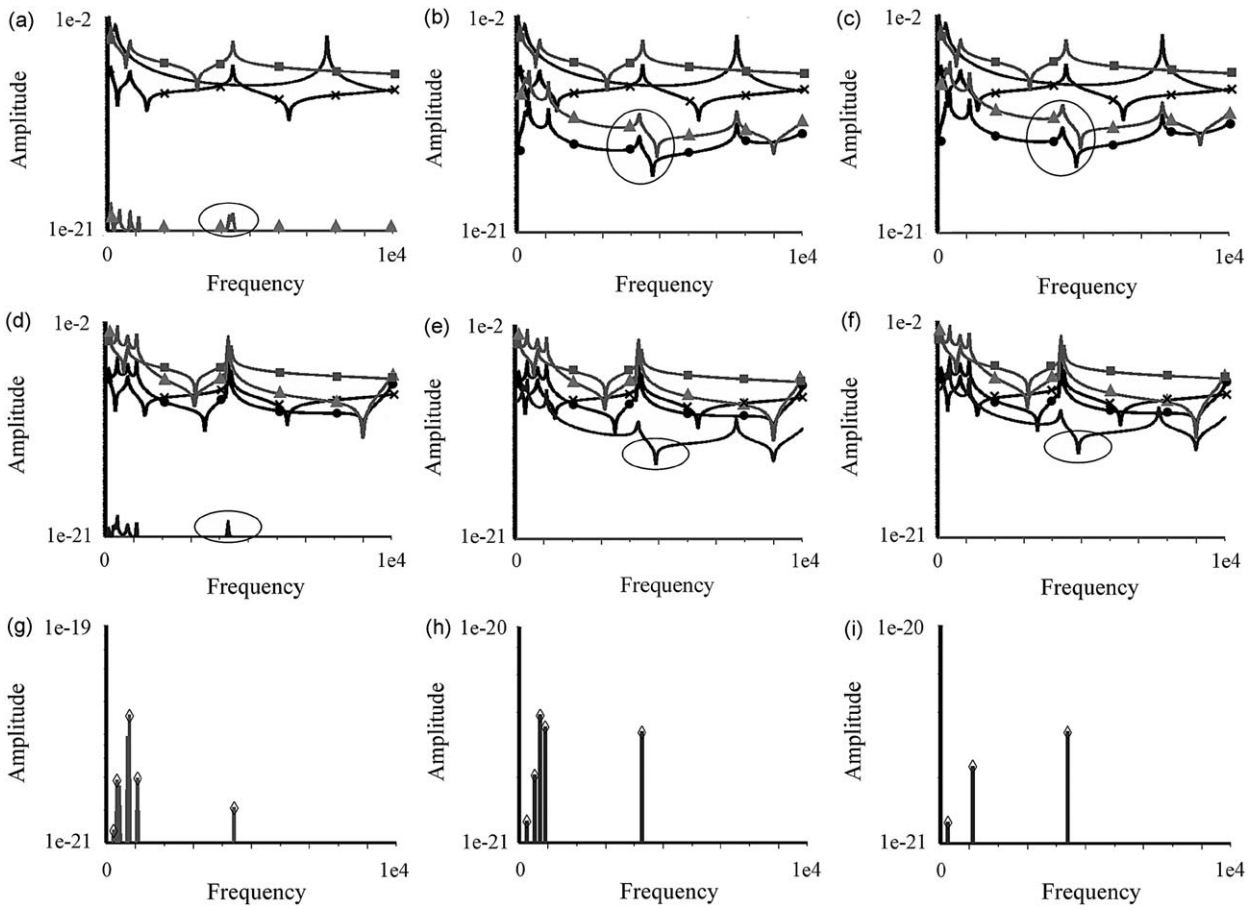


**Fig. 6.** Off-line amplitude vs. frequency (Hz) plots with torsional excitation on bearing 1 and responses on bearing 2. (a) Healthy shaft, torsional excitation around *X*-axis. (b) Open incipient crack, torsional excitation around *X*-axis. (c) Open deep crack, torsional excitation around *X*-axis. (d) Healthy shaft, torsional excitation around *Y*-axis. (e) Open incipient crack, torsional excitation around *Y*-axis. (f) Open deep crack, torsional excitation around *Y*-axis. (g) Healthy shaft, torsional excitation around *Z*-axis. (h) Open incipient crack, torsional excitation around *Z*-axis. (i) Open deep crack, torsional excitation around *Z*-axis. $U_x$ (◇), $U_y$ (**X**), $U_z$ (●), $T_x$ (——), $T_y$ (▲), $T_z$ (■).

and the axial response were also sensitive to cracking if a torsional excitation about the *Y*- and *Z*-axes, respectively, could be applied (Figs. 6(d)–(i)).

### 3.2.2. *Harmonic analysis at 5000 rev/min (on-line)*

When the shaft was rotating and a torsional excitation was applied, the location of the crack (top closed, bottom open) influenced the vibratory response by a small amount in the axial direction; an example of this situation is shown in Figs. 7(f) and (g). In general, the sensitivity to cracks increased when a torsional excitation was applied, and the combination of a torsional excitation and shaft rotation resulted in more options in the response data for detecting a crack than in the non-rotating shaft. The torsional response ($T_x$) and axial response were sensitive to damage using torsional excitations about either the *Y*- or *Z*-axis (Figs. 7(d)–(j)). Horizontal and axial responses were the most sensitive to cracks when a torsional excitation was applied about the *X*-axis (see Figs. 7(a)–(c)). Table 2(b) summarizes the results when torsional excitations were applied to the shaft.

## 3.3. *Special cases*

Two final numerical studies were conducted for a shaft rotation of 5000 rev/min: (1) multiple cracks, that is, two incipient cracks with the same orientation (open–open) and two incipient cracks with different orientations (closed–open) between bearing 1 and disc 1, and between disc 2 and bearing 2 and (2) combined faults, that is, a system with an open incipient crack at the mid-span with (a) misalignment and (b) a bent shaft. This latter study was important from a practical point of view because other faults are often present in rotating machines when cracks are being detected in the shafts.

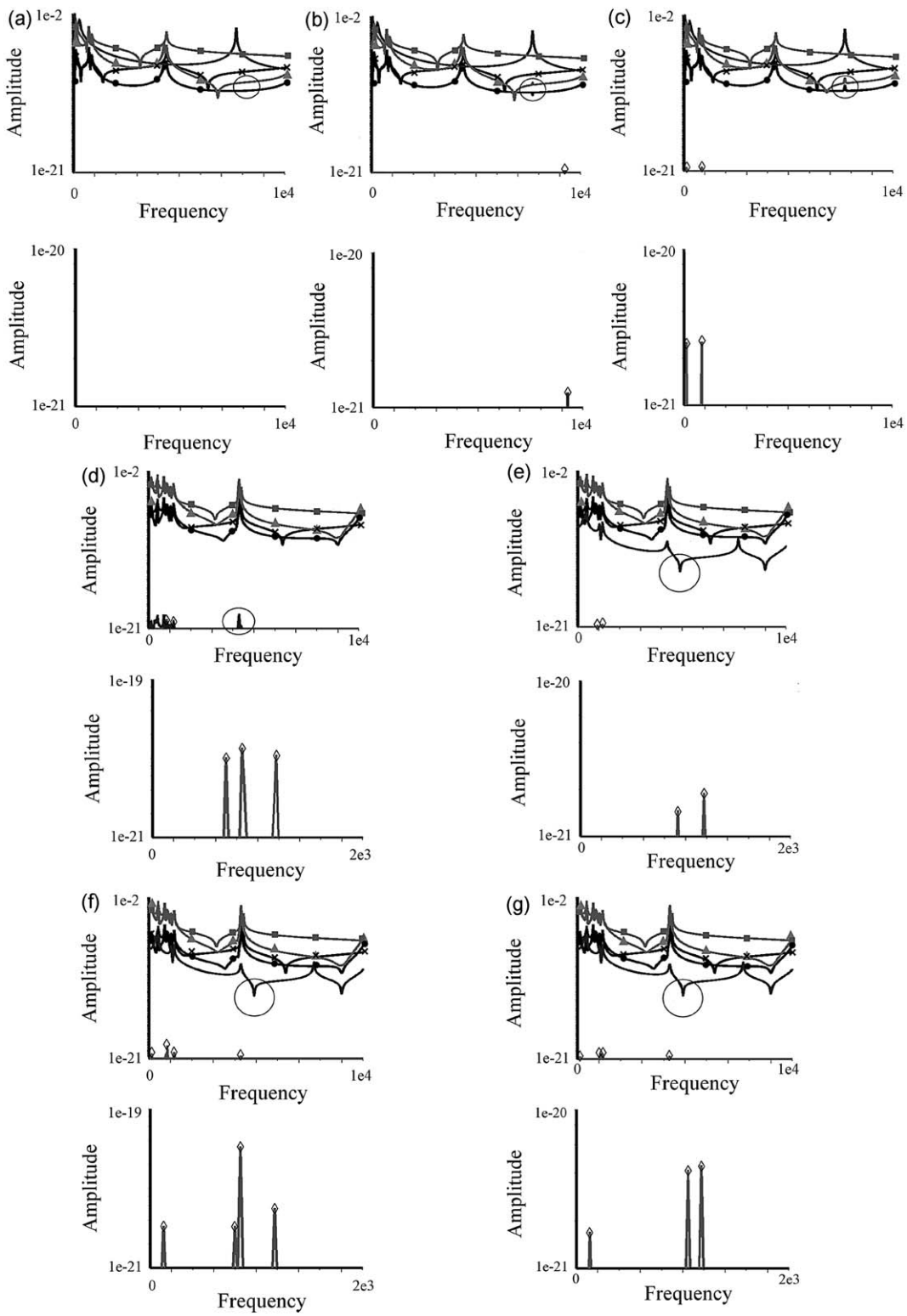


**Fig. 7.** On-line amplitude vs. frequency (Hz) plots with torsional excitation on bearing 1 and responses on bearing 2. (a) Healthy shaft, torsional excitation around *X*-axis. (b) Open incipient crack, torsional excitation around *X*-axis. (c) Open deep crack, torsional excitation around *X*-axis. (d) Healthy shaft, torsional excitation around *Y*-axis. (e) Open incipient crack, torsional excitation around *Y*-axis. (f) Open deep crack, torsional excitation around *Y*-axis. (g) Closed deep crack, torsional excitation around *Y*-axis. (h) Healthy shaft, torsional excitation around *Z*-axis. (i) Open incipient crack, torsional excitation around *Z*-axis. (j) Open deep crack, torsional excitation around *Z*-axis. When $U_x$ components are very small, they are plotted separately below other plots as in all the cases (a)–(j). $U_x$ (◇), $U_y$ (✖), $U_z$ (●), $T_x$ (——), $T_y$ (▲), $T_z$ (■).

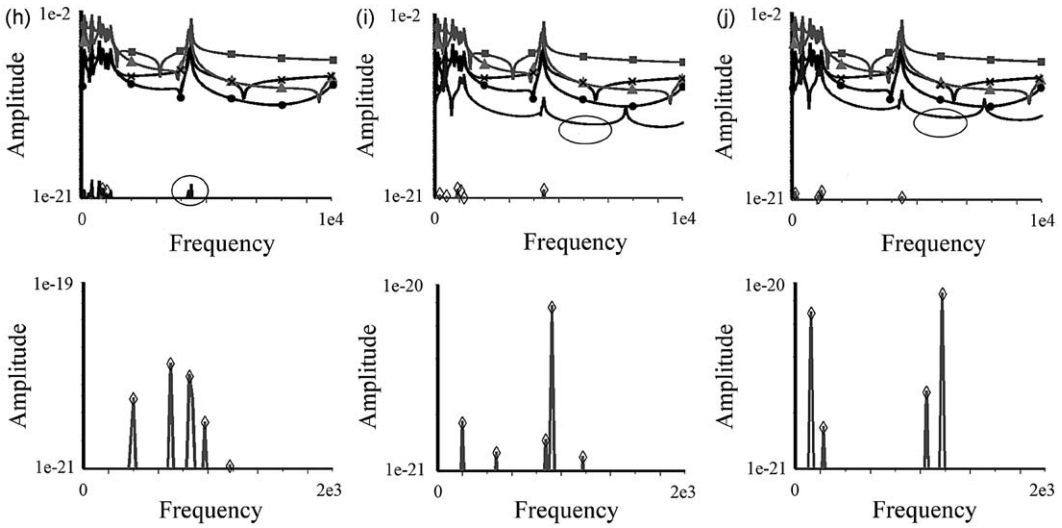


**Fig. 7.** (*Continued*)

### 3.3.1. Multiple cracks

Interesting results were obtained when two cracks were assumed and a horizontal excitation in a shaft rotating at 5000 rev/min was considered. The torsional vibratory response about the *X*-axis with two cracks exhibited a significantly different behavior with respect to the system containing only one crack at mid-span. The healthy system did not display a prominent torsional response ($T_x$). Also, the axial response for a system with two cracks exhibited differences in its frequency content and amplitudes depending on the crack orientations (healthy system and the system with only one crack did not have axial vibratory responses); see Figs. 8(a)–(d).

### 3.3.2. Combined faults

In Table 2(a), it was noted that when a system rotating with an incipient open crack was vertically excited, the system exhibited two different responses compared with a healthy shaft in the torsional ($T_x$) and axial components. Figs. 9(a)–(d) show that it was possible to distinguish between different kinds of faults when the faults occurred together. When there was misalignment or a bent shaft, all of the six responses changed with the most evident changes being in the axial response; moreover, resonance peaks appeared due to misalignment effects. Based on these results, it was concluded that good maintenance overhaul programs in machinery are critical to avoid the situation where a crack is masked by misalignment or a bent shaft. For space reasons, plots with only misalignment or bent shaft are not presented; however, these two faults also changed the six responses, but in a different way with respect to the other scenarios discussed.

## 4. Experimental work

Several laboratory tests with the shaft not spinning and mounted on both the bearings of the MFS and on a foam surface (off-line tests), and with the shaft spinning mounted on the bearings of the MFS (on-line tests), were carried out to qualitatively validate the results from the numerical simulations. A crack on the shaft at the mid-span was studied in addition to other kinds of faults (e.g., imbalance and misalignment).

### 4.1. Experimental apparatus and instrumentation

The MFS with two ball bearings was the experimental apparatus. The shaft was also extracted from the MFS, placed on a foam surface, and tested in several ways to study the healthy and damaged shaft responses under free–free boundary conditions.

Multidimensional vibration response data were acquired with PCB accelerometers. For the off-line tests with the shaft mounted on the MFS, triaxial sensors (sensitivity: 1000 mV/*g*; and frequency range: 0.5–3000 Hz) were installed on both bearings and 3 shaft locations: between bearing 1 and disc 1; between discs; and between disc 2 and bearing 2 (see Fig. 10(a)). When the shafts were placed on a foam surface, the same kind of sensor was used but on the shaft ends. For the on-line tests, another kind of triaxial accelerometer (sensitivity: 100 mV/*g*; and frequency range: 0.5–5000 Hz) was installed on both bearings. Uniaxial sensors (sensitivity: 100 mV/*g*; and frequency range: 0.5–3000 Hz) were also installed but only on the shaft ends to perform a few off-line tests with the shafts placed on a foam surface.

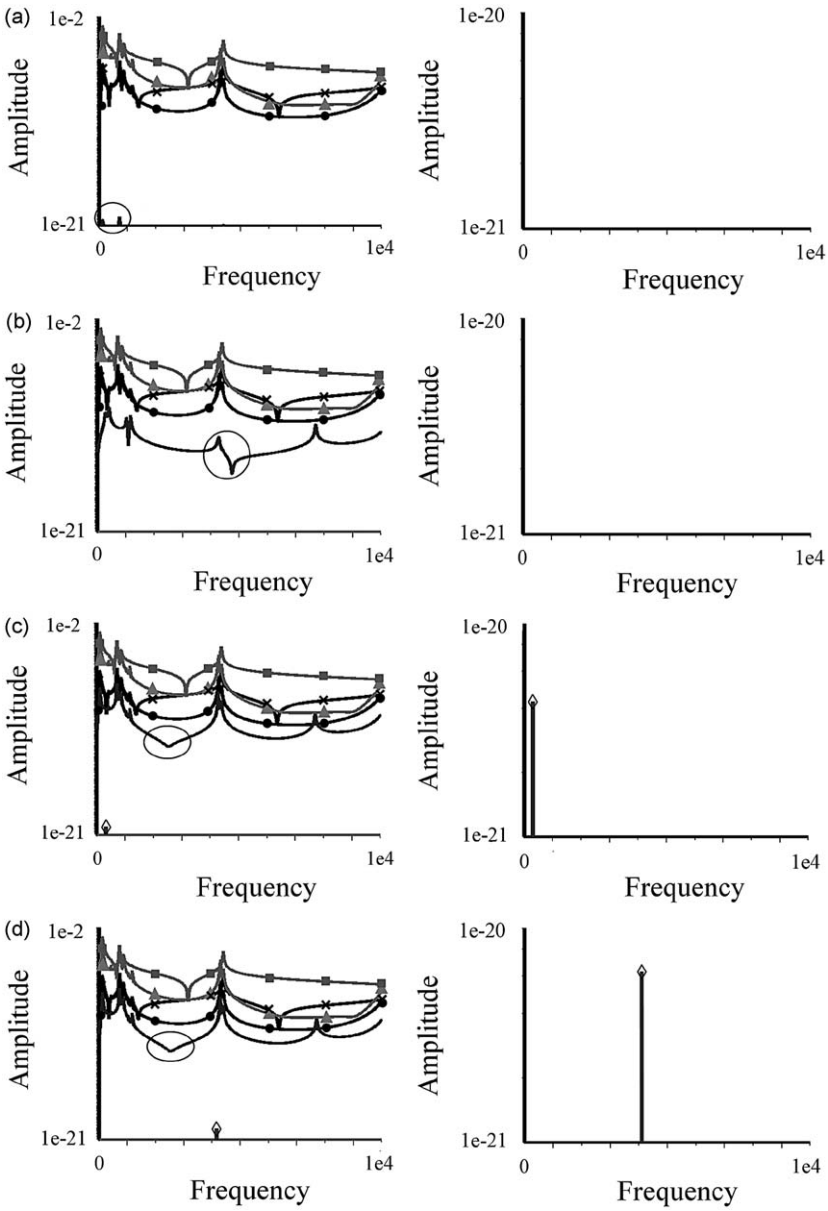


**Fig. 8.** On-line amplitude vs. frequency (Hz) plots with horizontal excitation on bearing 1 and responses on bearing 2. (a) Healthy shaft. (b) One open incipient crack at mid-span. (c) Two incipient cracks with the same orientation (open–open). (d) Two incipient cracks with different orientations (closed–open). When $U_x$ components are very small, they are plotted separately beside other plots as in all the cases (a)–(d). $U_x$ (◇), $U_y$ (✖), $U_z$ (●), $T_x$ (——), $T_y$ (▲), $T_z$ (■).

A medium sized modal impact hammer (PCB 2.25 mV/N) along with the sensors mentioned above for the off-line tests was used to collect frequency response functions (FRFs) in multiple directions. These FRFs were then used to estimate the natural frequencies and modal deflection shapes of the MFS. Two kinds of piezoelectric actuators were used to apply a variety of low-amplitude excitation forces in various directions and frequency bandwidths to one bearing housing or shaft end, and acceleration responses were measured at different locations. Fig. 10(b) shows the actuators used in this work. The first type of patch actuator applied a distributed stress in the transverse direction and the second disc actuator applied a more local excitation force (with the potential to add inertia to increase the level of that force). A power amplifier was used to produce adequate excitation levels.

The vibratory data were collected using a MATLAB®-based data acquisition system with delta-sigma A/D sampling (16+ channels VXI Agilent® 1432 system). MATLAB® algorithms were then applied to process and analyze data in near real time.

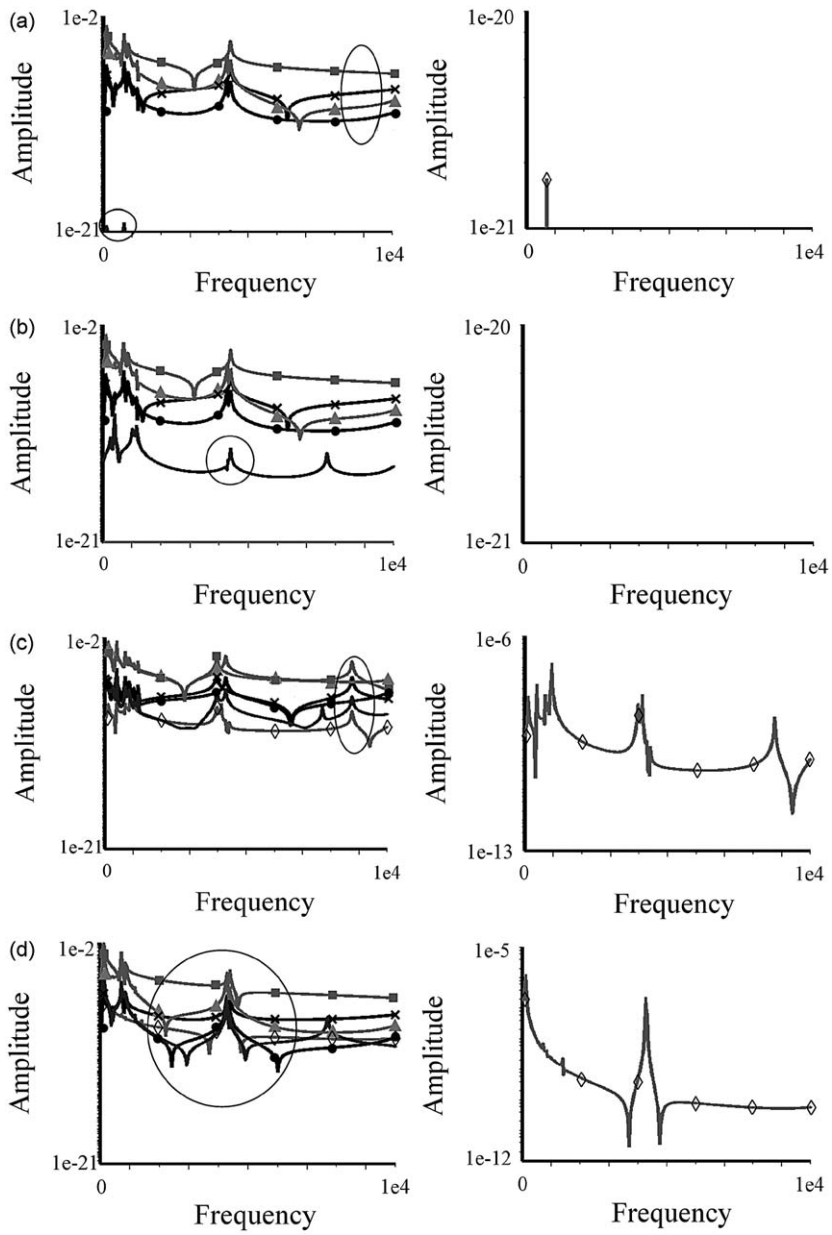


**Fig. 9.** On-line amplitude vs. frequency (Hz) plots with vertical excitation on bearing 1 and responses on bearing 2. (a) Healthy shaft. (b) Open incipient crack. (c) Open incipient crack and misalignment. (d) Open incipient crack and bent shaft. When $U_x$ components are very small, they are plotted separately beside other plots as in all the cases (a)–(d). $U_x$ (◇), $U_y$ (✖), $U_z$ (●), $T_x$ (——), $T_y$ (▲), $T_z$ (■).

The crack was machined using electrical discharge machining with a graphite electrode. The crack was very narrow (approximately 0.188 mm wide) with a depth equal to 12.5 percent of the shaft diameter. The specifications of the MFS are listed in Table 3.

### 4.2. Test procedure

Sensors were calibrated using a handheld shaker. The channel configuration for these tests is illustrated in Fig. 10(a). Only one input channel was used at a time when conducting active sensing experiments (impact hammer or actuator). When the shaft was rotating, only the vibration responses at the bearing locations using sensors 1 and 5 were measured.

Experiments using passive and active sensing were conducted to detect a crack at the shaft mid-span by measuring FRFs. A full complement of experiments was conducted to determine the effects of other faults (imbalance and misalignment) on the ability to detect a crack in the shaft.

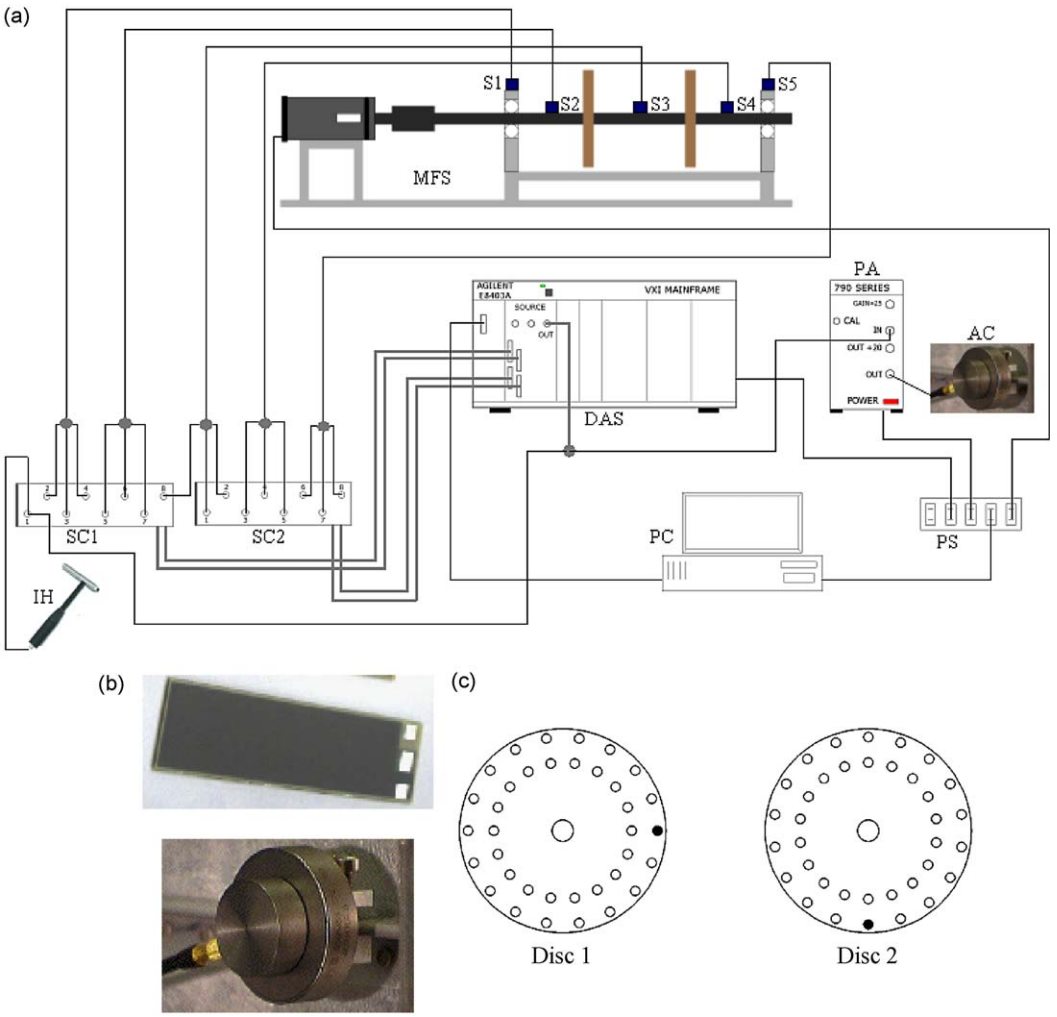


**Fig. 10.** (a) Connection of the diverse devices used: MFS—Machinery Fault Simulator; S—sensor; SC—signal conditioner; DAS—data acquisition system; PA—power amplifier; IH—impact hammer; AC—actuator; PS—power source; PC—personal computer. (b) Piezoelectric actuators: distributed piezoelectric patch and inertial (PCB Piezotronics®). (c) Mass imbalance locations seen from the motor (only one in each test); moderate imbalance = 120.84 gr cm; severe imbalance = 340.87 gr cm.

**Table 3**
Values for experimental configuration.

| | | |
|---|---|---|
| $E_{\text{shaft}} = 200\,\text{GPa}$ | $W_{\text{shaft}}\ (@\ L_{\text{shaft}}) = 8.01\,\text{N}$ | $L_{\text{disc}} = 0.016\,\text{m}$ |
| $v_{\text{shaft}} = 0.3$ | $W_{\text{shaft}}\ (@\ l_{\text{shaft}}) = 5.47\,\text{N}$ | $d_{\text{disc}} = 0.1524\,\text{m}$ |
| $\rho_{\text{shaft}} = 7800\,\text{kg/m}^3$ | $N_{\text{discs}} = 2$ | $W_{\text{disc}} = 6.01\,\text{N}$ |
| $L_{\text{shaft}} = 0.535\,\text{m}$ | $E_{\text{disc}} = 70\,\text{GPa}$ | $w_d = 0.145\,\text{m}$ |
| $l_{\text{shaft}} = 0.365\,\text{m}$ | $v_{\text{disc}} = 0.345$ | $t_{\text{crack}} = 0.188\text{e}{-3}\,\text{m}$ |
| $d_{\text{shaft}} = 0.015875\,\text{m}$ | $\rho_{\text{disc}} = 2700\,\text{kg/m}^3$ | $p/d_{\text{shaft}} = 0.125$ |

Both rectangular and Hanning windowed actuation signals were used to drive the actuators to determine the effects of these windows on the FRFs. Tests were carried out in the non-rotating and rotating operational conditions to determine the sensitivity of the measured active FRFs to the presence of a crack as well as the sensitivity of the FRFs to these cracks in the presence of vibrations induced due to rotordynamic forces and moments.

The MFS was tested several times for the same configuration to ensure that the experimental results were repeatable. Note that variability due to environmental factors, component parameters, and changes in boundary conditions is a leading cause of false positive indications of faults or low probabilities of detection in damage detection methods for machinery.

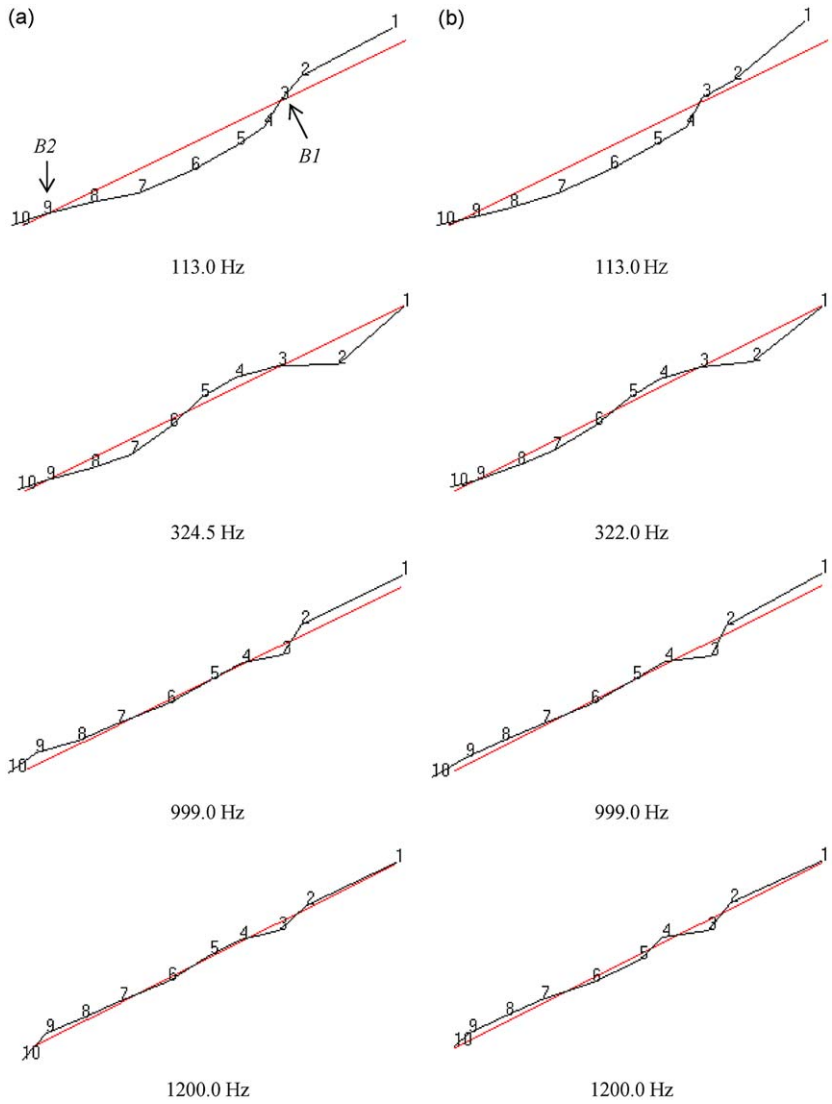


**Fig. 11.** Experimental modal shapes and natural frequencies: (a) healthy shaft and (b) cracked shaft.

### 4.3. Experimental results and analysis

Experiments were performed to estimate the natural frequencies and modal shapes of the MFS. An impact hammer was utilized together with accelerometers to obtain FRFs, which indicated the modal frequencies and modal shapes. Fig. 11 summarizes some of the modal parameters that were extracted from the data using the quadrature (peak-pick) method. The points marked with the number 3 represent bearing 1 (inboard) and number 9 represents bearing 2 (outboard). These results indicated that the presence of a crack did not produce significant changes in the natural frequencies and modal shapes.

#### 4.3.1. Off-line tests using impact hammer

The first set of tests using an impact hammer was performed to compare the responses of the healthy shaft and system with the responses obtained under different kinds of mass imbalance (see Fig. 10(c)). Fig. 12(a) shows that imbalance caused a change in the measured frequency response between a force applied on bearing 2 in the axial direction and response measured in the horizontal direction on bearing 1. It was also evident that the imbalance location and orientation did not have a significant effect on the static vibratory response. When the imbalance mass was moved, the response was similar. The effects of the mass imbalance magnitude are shown in Fig. 12(b). Different vibratory amplitudes were obtained when the imbalance magnitude changed and bearing 2 was axially excited. These tests showed that when the system was off-line, imbalance could be detected but its location and orientation could not be determined.

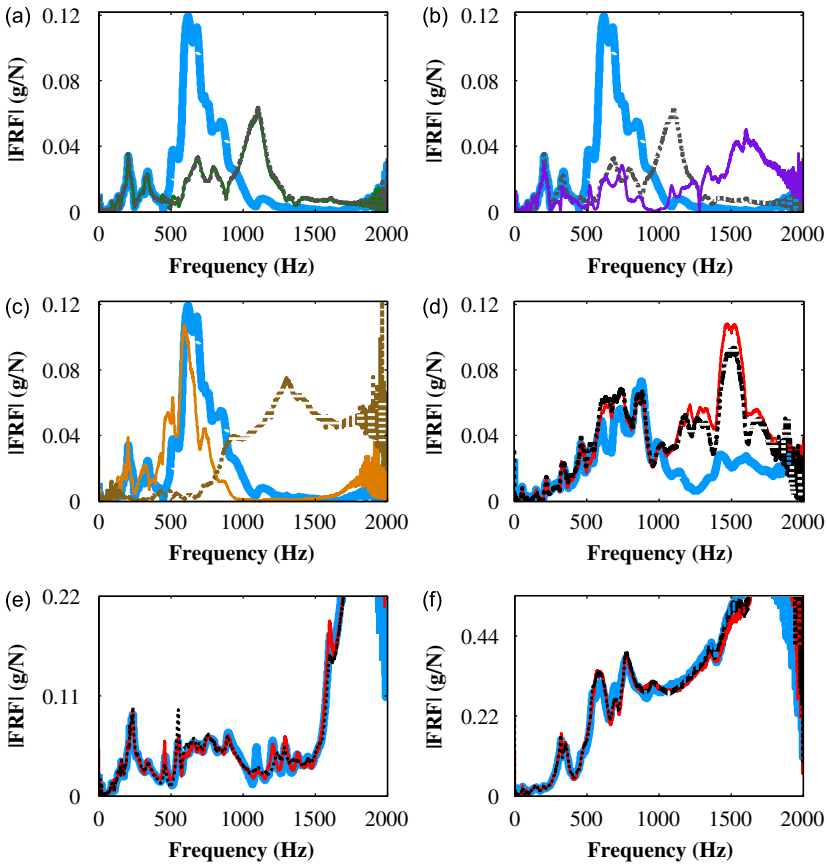


**Fig. 12.** Magnitude of the frequency response functions for various shaft and excitation configurations. (a) Healthy shaft (——) vs. severe imbalance in disc 1 (– – – –) and severe imbalance in disc 2 (——). Impact on bearing 2 with axial orientation and horizontal responses on bearing 1. (b) Healthy shaft (——) vs. moderate imbalance in disc 1 (——) and severe imbalance in disc 1 (– – – –). Impact on bearing 2 with axial orientation and horizontal responses on bearing 1. (c) Healthy shaft (——) vs. moderate misalignment (——) and severe misalignment (– – – –). Impact on bearing 2 with axial orientation and horizontal responses on bearing 1. (d) Healthy shaft (——) vs. cracked shaft, $\theta_m = 90^\circ$ (——) and cracked shaft, $\theta_m = 270^\circ$ (- - - -). Impact on bearing 1 with vertical orientation and axial responses on bearing 2. (e) Healthy shaft (——) vs. cracked shaft, $\theta_m = 90^\circ$ (——) and cracked shaft, $\theta_m = 270^\circ$ (- - - -). Impact on bearing 1 with horizontal orientation and axial responses on bearing 2. (f) Healthy shaft (——) vs. cracked shaft, $\theta_m = 90^\circ$ (——) and cracked shaft, $\theta_m = 270^\circ$ (- - - -). Impact on bearing 1 with axial orientation and axial responses on bearing 2.

The effects of misalignment are shown in the Fig. 12(c), where different combined misalignment magnitudes were observed to produce different frequency responses. Moderate misalignment was defined as a parallel misalignment of 0.127 mm plus an angular misalignment of 0.254 mm, whereas severe misalignment corresponded to 0.254 and 0.4064 mm, respectively.

A cracked shaft was tested by changing the crack orientation: $\theta_m = 90^\circ$ (closed crack) and $\theta_m = 270^\circ$ (open crack). A vertical excitation produced different axial frequency responses between the MFS systems containing healthy and cracked shafts; however, the differences in measured response due to a crack orientation were relatively small (see Figs. 12(d)–(f)). These results are consistent with the simulation results.

### *4.3.2. Off-line tests using actuator*

To better control the excitation forcing function, piezoelectric actuators were then used. With this type of excitation force, the differences in vibratory responses that were measured could be associated with only damage and not variability in modal impact force. The shaft was first dismounted from the MFS, placed over a foam surface, and a uniaxial accelerometer was attached on one end of the shaft. A rectangular window swept excitation (from 0 to 2 kHz) was applied on the other end with a piezoelectric patch. The results shown in Figs. 13(a)–(c) indicated that if the vibration response was in the same orientation as the excitation that was measured, there were no significant changes in the horizontal and vertical response between the healthy and cracked shafts (with different crack orientations), but in the axial orientation there were significant differences. Consequently, the axial orientation of the excitation would be useful to detect damage.

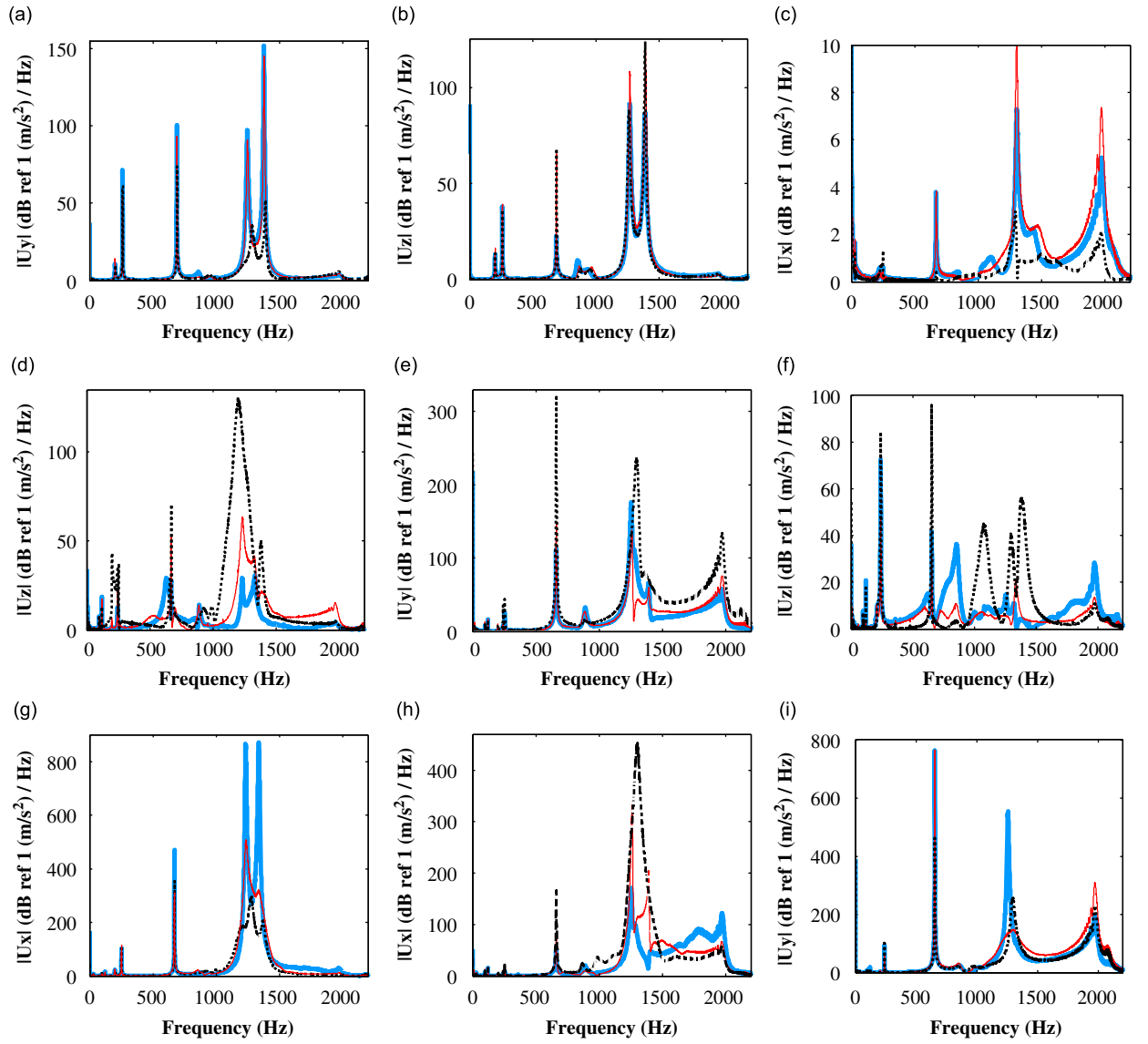


**Fig. 13.** Spectra of responses to off-line rectangular window swept excitation (from 0 to 2 kHz in 2 s) for various shaft and excitation configurations; shaft dismounted and placed on a foam surface. (a) Vertical excitation and vertical response (using uniaxial accelerometer). (b) Horizontal excitation and horizontal response (using uniaxial accelerometer). (c) Axial excitation and axial response (using uniaxial accelerometer). (d) Vertical excitation and horizontal response (using triaxial accelerometer). (e) Horizontal excitation and vertical response (using triaxial accelerometer). (f) Axial excitation and horizontal response (using triaxial accelerometer). (g) Vertical excitation and axial response (using triaxial accelerometer). (h) Horizontal excitation and axial response (using triaxial accelerometer). (i) Axial excitation and vertical response (using triaxial accelerometer). Healthy shaft (——); cracked shaft, $\theta_m = 90^\circ$ (——); cracked shaft, $\theta_m = 270^\circ$ (- - - -).

The same tests were performed with a triaxial accelerometer instead of the uniaxial device. Figs. 13(d)–(i) show the importance of using triaxial sensors because the responses in different orientations when the excitation was provided in a specific orientation exhibited more differences in the data for detecting damage because of coupling between the DOF in the shaft. The principal changes are in the horizontal frequency response under vertical and axial excitations, and axial frequency response under vertical and horizontal excitations. When the shaft was dismounted it was possible to measure changes in the vibratory response for the different crack orientations (when the crack was on the bottom, the change in response due to the crack was more evident).

Additionally, tests with the shaft mounted on the MFS were performed for both rectangular and Hanning window excitations with the piezoelectric inertial actuator. Forces in different orientations were applied using rectangular window swept excitations; however, the axial orientation was found to be the most sensitive to cracks in the shaft. In Fig. 14(a), the results are shown for an axial excitation on bearing 1 that produced different vibratory amplitudes and resonances for the healthy and cracked shafts; whereas very similar responses for both shafts were obtained when the excitation was vertical,

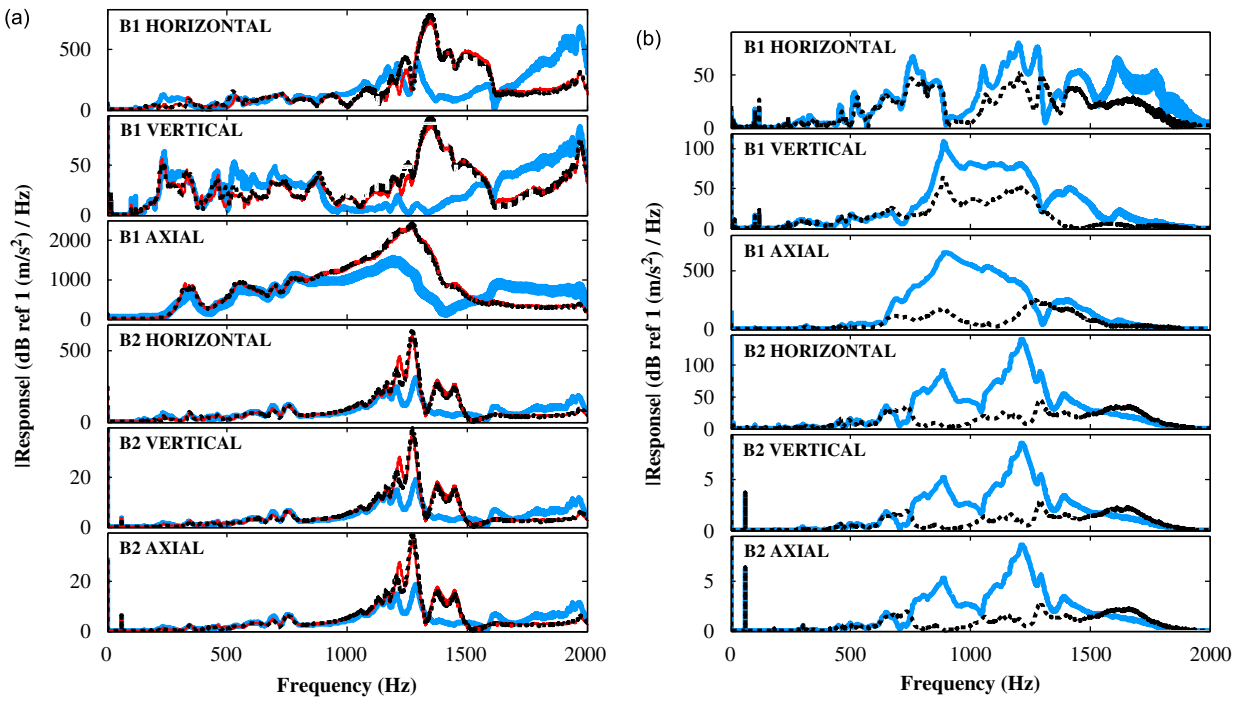


**Fig. 14.** Spectra of responses to off-line swept excitation (from 0 to 2 kHz in 2 s) on bearing 1. (a) Axial rectangular window swept excitation. (b) Vertical Hanning window swept excitation. Healthy shaft (——); cracked shaft, $\theta_m = 90^\circ$ (——); cracked shaft, $\theta_m = 270^\circ$ (- - - -).

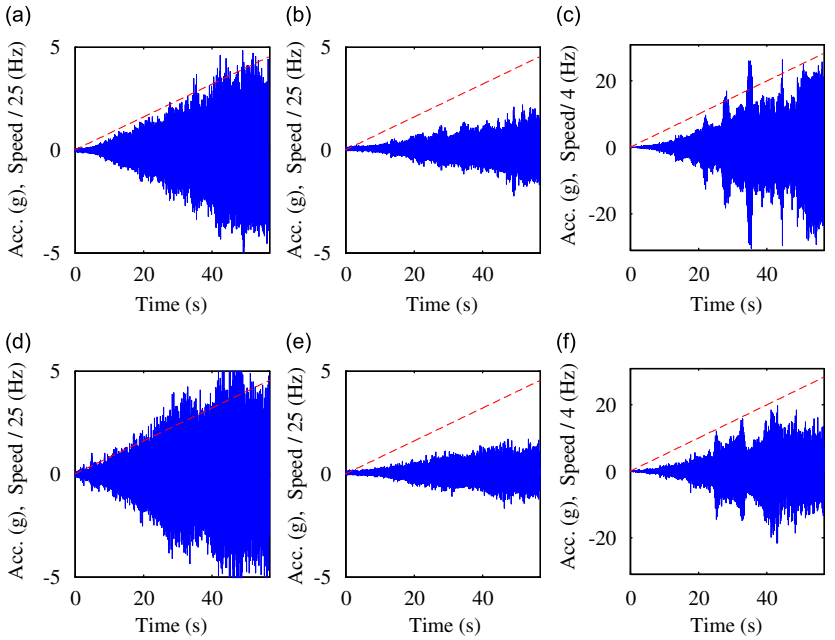


**Fig. 15.** Bearing 1 responses during a speed sweep (shaft run-up). (a) Healthy shaft, horizontal response. (b) Healthy shaft, vertical response. (c) Healthy shaft, axial response. (d) Cracked shaft, horizontal response. (e) Cracked shaft, vertical response. (f) Cracked shaft, axial response. Acceleration (——), speed (- - - -).

but in the interests of brevity those plots are not presented. As mentioned in the numerical simulations and shown in the tests using the modal hammer, the crack orientation did not have a significant effect on the response of the non-rotating shaft that was mounted on the MFS.

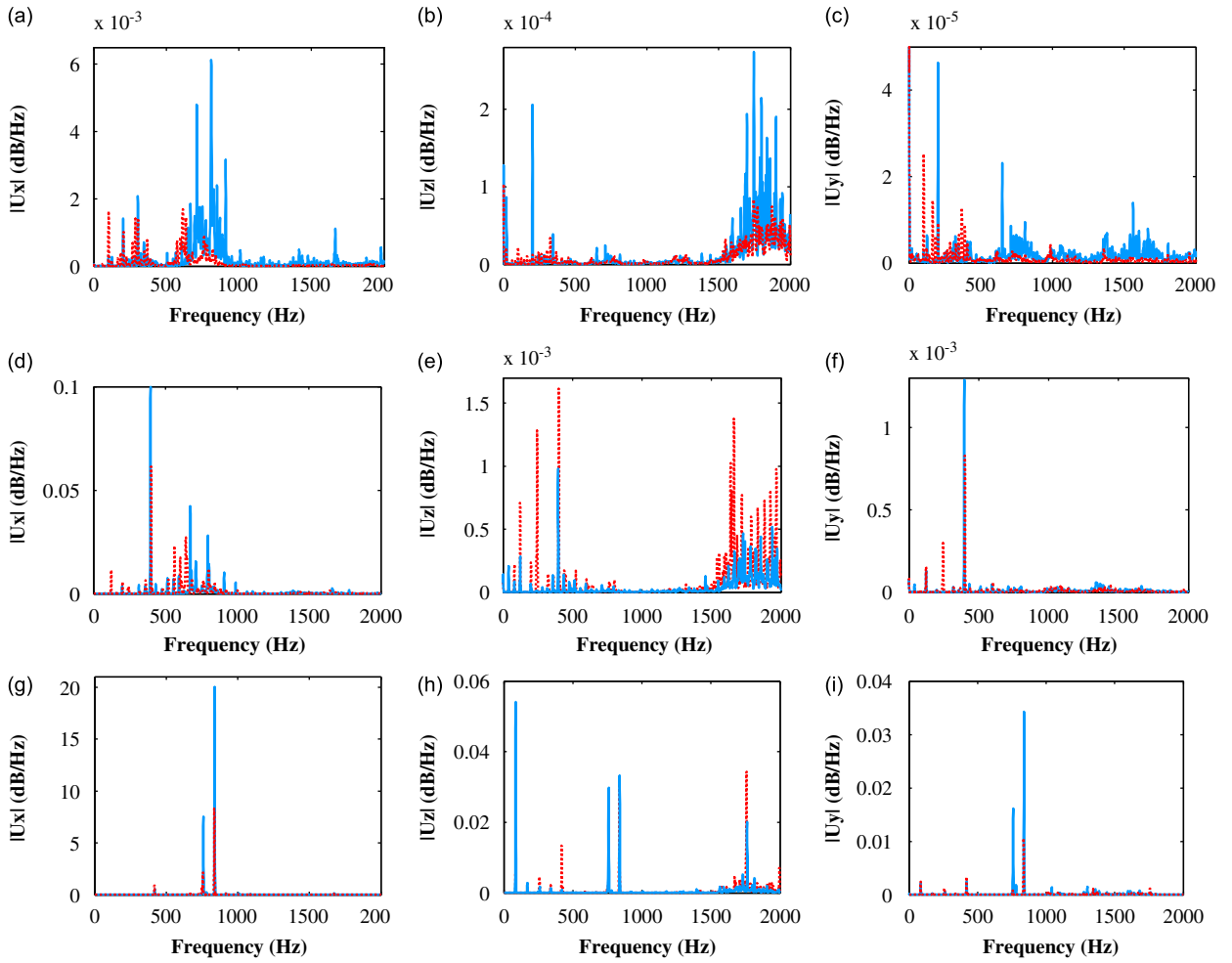


**Fig. 16.** Power spectral densities of axial, horizontal, and vertical responses on bearing 2 to rectangular windowed axial excitations on bearing 1 for various operating speeds. Row 1: (a)–(c), 1200 rev/min; row 2: (d)–(f), 2400 rev/min; and row 3: (g)–(i), 5100 rev/min. Column 1: (a), (d), and (g), axial responses; column 2: (b), (e), and (h), horizontal responses; and column 3: (c), (f), and (i), vertical responses. Healthy shaft (——); cracked shaft (– – –).

When a Hanning window excitation was applied, the sensitivities of the measured responses to cracking were different. For a Hanning window excitation in the axial orientation, there were no significant differences due to cracking in the bearing responses. The vertical excitation provided the most sensitivity response data for detecting cracks when a Hanning window was used; see Fig. 14(b). Each of these tests was repeated to ensure that the results were reproducible.

*4.3.3. On-line tests with and without actuator*

Several tests were also conducted when the shaft was rotating. First, speed sweeps during start-up without any external excitation were measured for the healthy and cracked shafts. The highest operational speed reached was 6800 rev/min at 56.7 s and the vibratory response was measured on the bearings. In Fig. 15, it was evident that similar responses for the healthy and cracked shafts in the horizontal (Figs. 15(a) and (d)) and vertical (Figs. 15(b) and (e)) directions were measured. Only the axial response exhibited a significant difference for these two cases, where the prominent amplitude peak for the healthy shaft at 35 s (4197.53 rev/min), which corresponds to $0.75\omega_c$ (first critical speed is 5611.07 rev/min), was inhibited due to the crack presence (see Figs. 15(c) and (f)). The axial response was the most sensitive to cracking when the shaft was spinning without external excitation and a torque sensor could not be implemented on the system. This result is consistent with the numerical simulations.

A piezoelectric inertial actuator was then used to excite bearing 1 (rectangular window swept excitation) in the axial direction while the shaft was spinning at constant speed. The frequency range of the excitation was from 0 to 2 kHz and 3 different constant operation speeds were studied: 1200, 2400, and 5100 rev/min. The results indicated that the axial excitation helped to detect damage when the shaft rotated at a constant speed; however, the ability to detect cracks depended on the operational speed. At 1200 rev/min the axial and vertical responses showed significant differences due to cracking (Figs. 16(a)–(c)); at 2400 rev/min the axial and horizontal responses showed even greater sensitivity to cracking

(Figs. 16(d)–(f)); at 5100 rev/min the data were complicated to detect the crack and only the horizontal response provided a clear indication near 410 Hz that the shaft was cracked (Figs. 16(g)–(i)). These results correlate well with the numerical simulation results previously presented in Figs. 4(d)–(f).

## 5. Conclusions

In this work, numerical and experimental results showed that the natural frequencies and mode shapes do not vary significantly when a transverse crack appears in the shaft of a rotordynamic system; therefore, active sensing was necessary to detect the damage. Exhaustive numerical simulations considering many different scenarios were carried out to determine measurements that most clearly detected cracking using external excitations. Torsional, transverse, and axial excitations were implemented on a bearing and all the six vibratory responses were measured on the opposite bearing considering both systems off-line and on-line. Systems simulating a healthy shaft, open incipient crack, open deep crack, and closed deep crack were analyzed; and additionally the effects of multiple cracks and combined faults (system with crack and misalignment, as well as a crack and bent shaft) were also briefly studied. The numerical results demonstrated the complexity of the crack detection problem when the system was off-line and axially excited; however, the sensitivity of measurements to cracks increased when using a transverse excitation and improved even further using a torsional excitation. Furthermore, it was seen that crack orientation does not have influence on the vibratory response when a non-rotating shaft was considered.

Several options for detecting cracks were identified when the shaft was rotating, transverse excitations were incorporated, and the torsional response ($T_x$) as well as the axial response were analyzed; these two responses were also useful to detect cracking when a torsional excitation was used but in non-realistic orientations (about the *Y*- and *Z*-axes). Nevertheless, horizontal and axial responses would be the most useful orientations for a practical torsional excitation scenario (about *X*-axis).

Two simultaneous cracks in the rotating system produced revealing torsional response ($T_x$) and axial response using a horizontal excitation, and the mutual cracks' orientations changed the frequency at which the axial amplitude peak appeared. Simulations predicted that the detection of cracks would be complicated by other faults, such as misalignment and bent shafts, because these two faults produced different torsional response ($T_x$) and axial response with respect to the system without faults (healthy); however, crack detection was possible through the use of active sensing because the torsional response ($T_x$) and the axial response obtained for combined faults (crack and misalignment or crack and bent shaft), or only either misalignment or a bent shaft, exhibited different characteristics with respect to the torsional response ($T_x$) and axial response of the rotating shaft with only a crack. The misalignment and bent shaft faults (with or without a crack) changed all the six responses with respect to the system without faults, whereas a system with a cracked shaft did not cause all six responses to change (no more than three responses were modified by the crack). This finding is relevant to industrial machinery because false alarms due to cracked shafts could be avoided.

Laboratory tests showed the imbalance and misalignment effects when the non-rotating shaft was mounted on the experimental apparatus and axially excited with an impact hammer; moreover, it was validated that the transverse crack orientation did not influence the results. Two options to detect cracks in a non-rotating shaft were discussed. In the first method, it is necessary to dismount the shaft from the machinery, place it on a foam surface, excite it on one end in any orientation, and analyze the vibratory responses in different orientations with respect to the excitation. Changes between the healthy and cracked non-rotating shafts could be distinguished and the crack could be located because its different orientations produce different responses. In the second option, it was possible to diagnose cracks with the shaft mounted in the system, but an axial rectangular window excitation or vertical Hanning window excitation was necessary. The crack orientation did not have an effect as demonstrated in the numerical work and tests with an impact hammer. Finally, experimental on-line tests validated several of the numerical simulation findings such as the utility of the axial response observed in rotating shafts without any excitation and the possibilities of detecting damage in a rotating shaft that is excited externally.

## Acknowledgments

The authors gratefully acknowledge the support offered by Consejo Nacional de Ciencia y Tecnología (CONACYT).

## Appendix

*Elements used in the numerical model*

The ANSYS® model that was developed uses beam189 elements to represent the shaft and discs and combin14 to represent the bearings and foundation. Beam189 is a 3-noded quadratic element with 6–7 DOF and is suitable for modeling slender to moderately thick linear structures. Timoshenko beam theory is the basis for the mechanical characteristics of this element, which incorporates shear deformation effects. Translations at each node in three Cartesian directions and

rotations in three directions are included in the model; a seventh DOF (warping magnitude) could also be considered. By including stress-stiffening terms, beam189 enables the study of flexural, axial, and torsional dynamic response and stability problems. Although creep and plasticity models can also be incorporated, linear elastic constitutive laws will be assumed in the initial model. Beam189 can be used with any beam cross-section and the cross-section associated with this element type can be a built-up section referencing more than one material.

Combin14 is an element with longitudinal or torsional DOFs in 1-D, 2-D, or 3-D. The longitudinal spring-damper is a uniaxial tension-compression element with up to 3 DOF per node: translations in the nodal *X*, *Y*, and *Z* directions. The torsional spring-damper is a purely rotational element with 3 DOF at each node: rotations about the nodal *X*-, *Y*-, and *Z*-axes. This element has no mass and the spring or the damping characteristics may be easily removed from the element.

*Characteristics of the final numerical model*

The model consists of 12 key points, 11 lines (6 elements per line), 94 elements (66 elements type beam189 and 28 elements type combin14), and 161 nodes; see Fig. 1(c). The discs were modeled as simple rigid body solid elements with the appropriate material properties (aluminum discs in the case of the MFS). Different stiffness and damping values in the two bearings and foundation in seven orientations (*YZ*, *ZZ*, *ZY*, *YY*, *YX*, *XX*, and *XY*) can be considered (see Figs. 1(d) and (e)). The stiffness and damping values within the combin14 elements were selected based on the geometry of the supports using strength of materials concepts. Cracks were modeled using notches inserted in the respective lines along the shaft to modify the cross-sectional area. Imbalance was considered using skewed centers of mass in the discs. Parallel, angular, or combined misalignment at bearing 2 (outboard) can be taken into account. Analysis with a bent shaft at the mid-span can be also performed.

The gravitational field was modeled and the shaft can be static or rotating. Furthermore, the Coriolis effects as well as the so-called "spin softening" (radial stiffness reduction in the element) were taken into account for analyses with shaft spinning.

The proposed model enables static, free response (modal), harmonic loading, and transient (dynamic) forced response analysis. The available outputs include deformations, strains, natural frequencies, modal shapes, and plots of amplitude vs. frequency, phase vs. frequency, time vs. amplitude, as well as Campbell diagrams and orbits for the rotating shaft. An IBM® AIX workstation was utilized for conducting these simulations and analyzing the resultant data. Summarizing, this model allows the consideration of several conditions: (1) system with healthy shaft; (2) system with damaged shaft with 1, 2, or 3 simultaneous transverse cracks in different locations and with different depths ($p/d_{\text{shaft}} = 0.125, 0.25$, or 0.50); see Fig. 1(e); (3) system with mass imbalance in the first or second disc (any mass magnitude); (4) system with angular, parallel, or combined misalignment at bearing 2 (0.254 mm is the angular, parallel, or combined misalignment value); (5) system with bent shaft at mid-span (0.254 mm is the magnitude of this bending); and (6) system with damaged shaft with 1, 2, or 3 simultaneous transverse cracks and: (a) imbalance in the first or second disc, (b) angular, parallel, or combined misalignment at bearing 2, or (c) bent shaft at mid-span.

*Consideration of a crack in the shaft of the numerical model*

Transverse cracks (always closed or open) in different locations of the shaft were considered by varying the cross-sectional area, moment of inertia, polar moment of inertia, and geometric center in the specific cracked elements (see Figs. 1(f) and (g)). In this study, the deflection of the horizontal shaft due to gravity is insignificant compared with the whirl, so that a crack is always closed or open. The crack thickness machined into the shaft used for experimentation was 0.188 mm; therefore, the cracked line(s) thickness was selected to be the same in the ANSYS® model. The equations obtained from Fig. 1(g) to estimate the important variation of the moment of inertia in the cracked sections are written below; moreover, considering the experimental shaft dimensions and those equations (Eqs. (1)–(5)), the parameters in Table 1 are obtained.

Moment of inertia of the damaged circular section:

$$I_f = I_i - I_{as} + I_{ts} \tag{1}$$

Moment of inertia of the healthy circular section:

$$I_i = \frac{\pi r^4}{4} \tag{2}$$

Moment of inertia of the angular sector OADCO:

$$I_{as} = \frac{r^4}{4}\left(\frac{\theta_f - \theta_i}{2} - \frac{\sin 2\theta_f - \sin 2\theta_i}{4}\right) \tag{3}$$

Moment of inertia of the triangular sector OABCO:

$$I_{ts} = \frac{(r-p)r^3}{12\cos\theta_m}[(\sin\theta_f)^3 - (\sin\theta_i)^3] \quad \text{for } \theta \neq \frac{n(\pi)}{2} \text{ with } n = 1,3,5,7,\ldots \tag{4}$$

$$I_{ts} = \frac{r(r-p)^3}{2}\cos\theta_i \text{ for } \theta = \frac{n(\pi)}{2} \text{ with } n = 1,3,5,7,\ldots \tag{5}$$

## References


[1] I.S. Zagretdinov, A.G. Kostyuk, A.D. Trukhnii, P.R. Dolzhanskii, Destruction of the 300 MW turbine-generator unit at the Kashira district power station: causes, consequences, and conclusions, *Thermal Engineering* 51 (2004) 345–355.
[2] D.A. Weisz, Analysis of the Tennessee Valley Authority Gallatin No. 2 unit turbine rotor burst. Mechanical analysis, in: *Proceedings of the Tribology Conference*, New York City, USA, December 1976, pp. 25–40.
[3] R. Abinger, F. Hammer, J. Leopold, Large-scale damage to a 330 MW steam turboset (in German), *Maschinenschaden* 61 (1988) 58–63.
[4] G. Sabnavis, R.G. Kirk, M. Kasarda, D. Quinn, Cracked shaft detection and diagnostics: a literature review, *Shock and Vibration Digest* 36 (2004) 287–296.
[5] C.A. Papadopoulos, A.D. Dimarogonas, Coupled vibration of cracked shafts, *Journal of Vibration and Acoustics* 114 (1992) 461–467.
[6] J.S. Rao, *Rotor Dynamics*, Wiley, New York, 1983 (re-issued 1991).
[7] D.E. Bently, Shaft crack detection in rotating machinery, in: *Proceedings of the 47th Meeting of the Mechanical Failures Prevention Group*, Virginia Beach, Virginia, USA, April 1993, pp. 1–27.
[8] A. Muszynska, Shaft crack detection, *Proceedings of the Seventh Machinery Dynamics Seminar*, Edmonton, Canada, 1982, pp. 4.0–4.49.
[9] L.R.K. Nilsson, On the vibrational behavior of a cracked rotor-bearing system, in: *Proceedings of the International Conference on Rotordynamic Problems in Power Plants*, Rome, Italy, September 1982, pp. 515–524.
[10] R. Gasch, A survey of the dynamic behaviour of a simple rotating shaft with a transverse crack, *Journal of Sound and Vibration* 160 (1993) 313–332.
[11] A.S. Sekhar, Vibration characteristics of a cracked rotor with two open cracks, *Journal of Sound and Vibration* 223 (1999) 497–512.
[12] A.K. Darpe, K. Gupta, A. Chawla, Dynamics of a two-crack rotor, *Journal of Sound and Vibration* 259 (2003) 649–675.
[13] J.E.T. Penny, M.I. Friswell, Simplified modelling of rotor cracks, in: *Proceedings of the International Conference on Noise and Vibration Engineering*, Leuven, Belgium, September 2002, pp. 607–615.
[14] J.C. Gómez-Mancilla, J.-J. Sinou, V.R. Nossov, F. Thouverez, A. Zambrano-Reyes, The influence of crack-imbalance orientation and orbital evolution for an extended cracked Jeffcott rotor, *Comptes Rendus Mécanique* 332 (2004) 955–962.
[15] J.C. Gómez-Mancilla, J.M. Machorro-López, Local resonance of crack-imbalance orientations and orbital evolution to detect mid-span rotor cracks: part 2, experimental validation, in: *Proceedings of the XXIII International Modal Analysis Conference*, Orlando, Florida, USA, January 2005, pp. 106–113.
[16] J.C. Gómez-Mancilla, J.M. Machorro-López, V.R. Nossov, Crack breathing mechanisms in rotor-bearings systems, its influence on system response and crack detection, in: *Proceedings of the Third International Symposium on Stability Control of Rotating Machinery*, Cleveland, Ohio, USA, September 2005, pp. 418–427.
[17] V.V. Kucherenko, J.C. Gómez-Mancilla, Bifurcations of an exactly solvable model of rotodynamics, *International Journal of Bifurcation and Chaos* 10 (2000) 2689–2699.
[18] S.M. Al-Said, M. Naji, A.A. Al-Shukry, Flexural vibration of rotating cracked Timoshenko beam, *Journal of Vibration and Control* 12 (2006) 1271–1287.
[19] J. Antoni, R.B. Randall, The spectral kurtosis: application to the vibratory surveillance and diagnostics of rotating machines, *European Journal of Mechanics A/Solids* 20 (2006) 308–331.
[20] J.-J. Sinou, A.W. Lees, A nonlinear study of a cracked rotor, *European Journal of Mechanics A/Solids* 26 (2007) 152–170.
[21] Y. Ishida, T. Inoue, Detection of a rotor crack using a harmonic excitation and nonlinear vibration analysis, *Journal of Vibration and Acoustics* 128 (2006) 741–749.